10
Methods of Radiation Detection

This chapter describes ways in which ionizing radiation can be detected and measured. Section 10.7 covers special methods applied to neutrons. In Chapter 12 we shall see how these techniques are applied in radiation dosimetry.

10.1
Ionization in Gases

Ionization Current

Figure 10.1(a) illustrates a uniform, parallel beam of monoenergetic charged particles that steadily enter a gas chamber across an area A with energy E and come to rest in the chamber. A potential difference V applied across the parallel chamber plates P_1 and P_2 gives rise to a uniform electric field between them. As the particles slow down in the chamber, they ionize gas atoms by ejecting electrons and leaving positive ions behind. The ejected electrons can immediately produce additional ion pairs. If the electric field strength, which is proportional to V, is relatively weak, then only a few of the total ion pairs will drift apart under its influence, and a small current I will flow in the circuit. Most of the other ion pairs will recombine to form neutral gas atoms. As shown in Fig. 10.1(b), the current I can be increased by increasing V up to a value V_0, at which the field becomes strong enough to collect all of the ion pairs produced by the incident radiation and its secondary electrons. Thereafter, the current remains on a plateau at its saturation value I_0 when $V > V_0$.

Since it is readily measurable, it is important to see what information the saturation current gives about the radiation. If the fluence rate is $\dot{\Phi}$ cm^{-2} s^{-1}, then the intensity $\dot{\Psi}$ of the radiation (Section 8.8) entering the chamber is given by $\dot{\Psi} = \dot{\Phi}E$. If W denotes the average energy needed to produce an ion pair when a particle of initial energy E stops in the chamber, then the average number N of ion pairs produced by an incident particle and its secondary electrons is $N = E/W$. The average charge (either + or –) produced per particle is Ne, where e is the magnitude of the electronic charge. The saturation current I_0 in the circuit is equal to the product of Ne and $\dot{\Phi}A$, the total number of particles that enter the chamber per unit time. Therefore, we have

Atoms, Radiation, and Radiation Protection. James E. Turner

ISBN: 978-3-527-40606-7

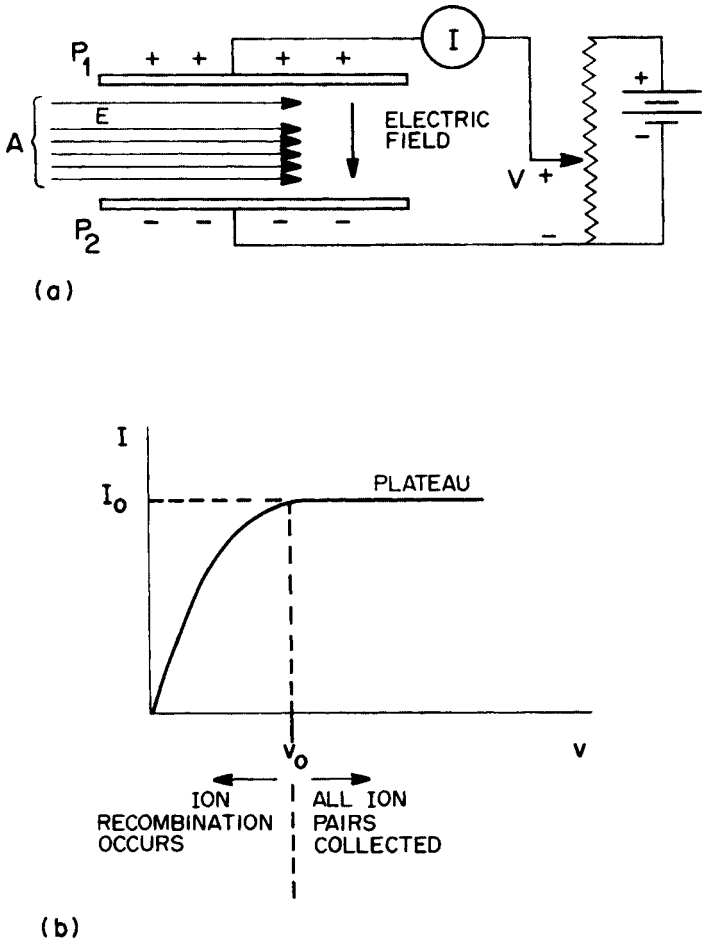

Fig. 10.1 (a) Monoenergetic beam of particles stopping in parallel-plate ionization chamber with variable potential difference V applied across plates P_1 and P_2 (seen edge on). (b) Plot of current I vs. V.

$$I_0 = Ne\dot{\Phi}A = \frac{e\dot{\Phi}AE}{W}. \tag{10.1}$$

It follows that

$$\dot{\Psi} = \dot{\Phi}E = \frac{I_0 W}{eA}, \tag{10.2}$$

showing that the beam intensity is proportional to the saturation current.

The important relationship (10.2) is of limited use, because it applies to a uniform, parallel beam of radiation. However, since the rate of total energy absorption in the chamber gas, $\dot{E}_{\text{abs}}$, is given by $\dot{E}_{\text{abs}} = \dot{\Psi}A$, we can write in place of Eq. (10.2)

$$\dot{E}_{\text{abs}} = \frac{I_0 W}{e}. \tag{10.3}$$

Thus, the saturation current gives a direct measure of the rate of energy absorption in the gas. The relationship (10.3) holds independently of any particular condition on beam geometry, and is therefore of great practical utility. Fortunately, it is the energy absorbed in a biological system that is relevant for dosimetry; the radiation intensity itself is usually of secondary importance.

Example

Good electrometers measure currents as small as 10^{-16} A. What is the corresponding rate of energy absorption in a parallel-plate ionization chamber containing a gas for which $W = 30$ eV per ion pair (eV ip^{-1})?

Solution

From Appendix B, 1 A = 1 C s^{-1}. Equation (10.3) gives

$$\dot{E}_{\text{abs}} = \frac{(10^{-16}\ \text{C s}^{-1}) \times 30\ \text{eV}}{1.6 \times 10^{-19}\ \text{C}} = 1.88 \times 10^{4}\ \text{eV s}^{-1}. \tag{10.4}$$

Ionization measurements are very sensitive. This average current would be produced, for example, by a single 18.8-keV beta particle stopping in the chamber per second.

W Values

Figure 10.2 shows W values for protons (H), alpha particles (He), and carbon and nitrogen ions of various energies in nitrogen gas, N_2. The values represent the average energy expended per ion pair when a particle of initial energy E and all of the secondary electrons it produces stop in the gas. The value for electrons, $W_\beta = 34.6$ eV ip^{-1}, shown by the horizontal line, is about the same as that for protons at energies $E > 10$ keV. W values for heavy ions, which are constant at high energies, increase with decreasing energy because a larger fraction of energy loss results in excitation rather than ionization of the gas. Elastic scattering of the ions by nuclei also causes a large increase at low energies.

The data in Fig. 10.2 indicate that W values for a given type of charged particle are approximately independent of its initial energy, unless that energy is small. This fact is of great practical significance, since it often enables absorbed energy to be inferred from measurement of the charge collected, independently of the identity or energy spectrum of the incident particles. Alternatively, the rate of energy absorption can be inferred from measurement of the current.

W values for many polyatomic gases are in the range 25–35 eV ip^{-1}. Table 10.1 gives some values for alpha and beta particles in a number of gases.

We have defined W as the average energy needed to produce an ion pair and expressed it in eV ip^{-1}. Since 1 eV = 1.60×10^{-19} J and the charge separated per ion pair is 1.60×10^{-19} C, it follows that W has the same numerical value when expressed either in eV ip^{-1} or J C^{-1} (Problem 13).

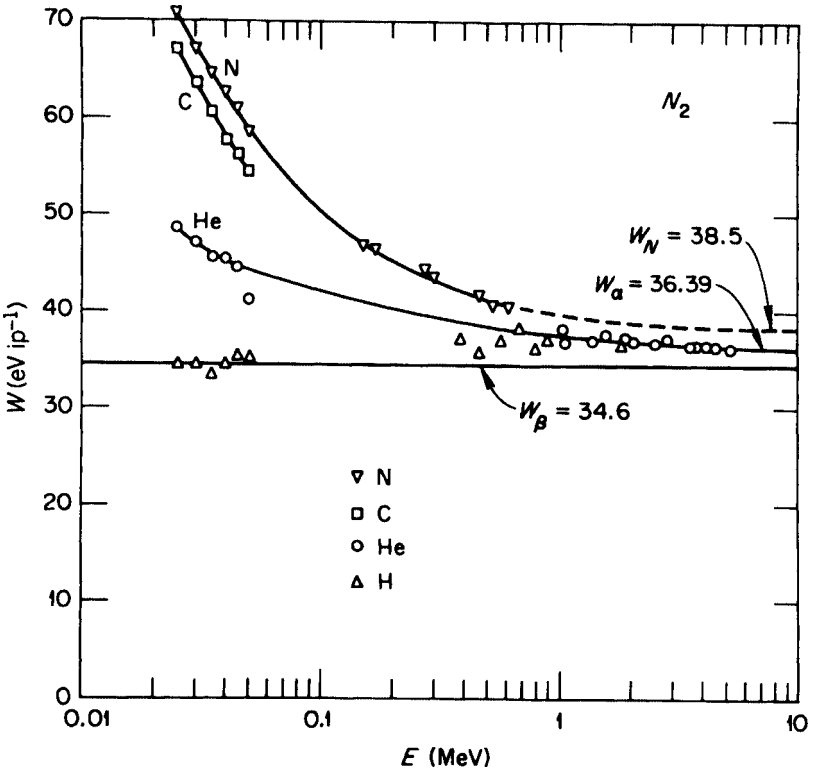

Fig. 10.2 *W* values for electrons, protons, alpha particles, carbon ions, and nitrogen ions in nitrogen gas as a function of initial particle energy *E*. The points represent experimental data, through which the curves are drawn. (Courtesy Oak Ridge National Laboratory, operated by Martin Marietta Energy Systems, Inc., for the Department of Energy.)

Table 10.1 *W* Values, W_α and W_β, for Alpha and Beta Particles in Several Gases

Gas	W_α (eV ip^{-1})	W_β (eV ip^{-1})	W_α / W_β
He	43	42	1.02
H_2	36	36	1.00
O_2	33	31	1.06
CO_2	36	33	1.09
CH_4	29	27	1.07
C_2H_4	28	26	1.08
Air	36	34	1.06

Ionization Pulses

In addition to measuring absorbed energy, a parallel-plate ionization chamber operated in the plateau region [Fig. 10.1(b)] can also be used to count particles. When a charged particle enters the chamber, the potential difference across the plates momentarily drops slightly while the ions are being collected. After collection, the potential difference returns to its original value. The electrical pulse that occurs during ion collection can be amplified and recorded electronically to register the particle. Furthermore, if the particle stops in the chamber, then, since the number of ion pairs is proportional to its original energy, the size of each pulse can be used to determine the energy spectrum. While such measurements can, in principle, be carried out, pulse ionization chambers are of limited practical use because of the attendant electronic noise.

The noise problem is greatly reduced in a proportional counter. Such a counter utilizes a gas enclosed in a tube often made with a fine wire anode running along the axis of a conducting cylindrical-shell cathode, as shown schematically in Fig. 10.3. The electric field strength at a distance r from the center of the anode in this cylindrical geometry is given by

$$\epsilon(r) = \frac{V}{r \ln(b/a)}, \tag{10.5}$$

where V is the potential difference between the central anode and the cylinder wall, b is the radius of the cylinder, and a is the radius of the anode wire. With this arrangement, very large field strengths are possible when a is small in the region near the anode, where r is also small. This fact is utilized as follows.

Consider the pulse produced by an alpha particle that stops in the counter gas. When the applied voltage is low, the tube operates like an ionization chamber. The number of ion pairs collected, or pulse height, is small if the voltage is low enough

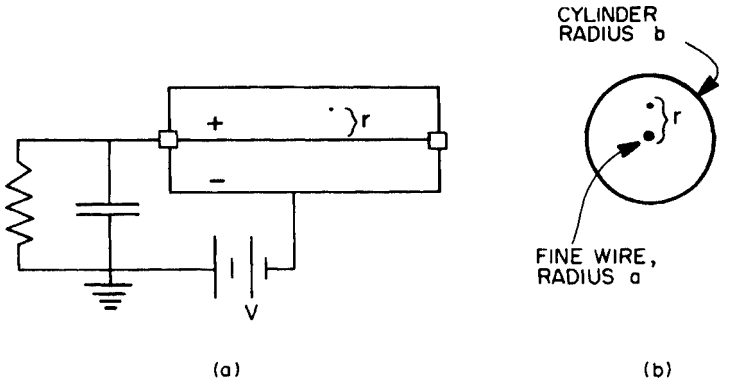

Fig. 10.3 (a) Schematic side view and (b) end view of cylindrical proportional-counter tube. Variation of electric field strength with distance r from center of anode along cylindrical axis is given by Eq. (10.5).

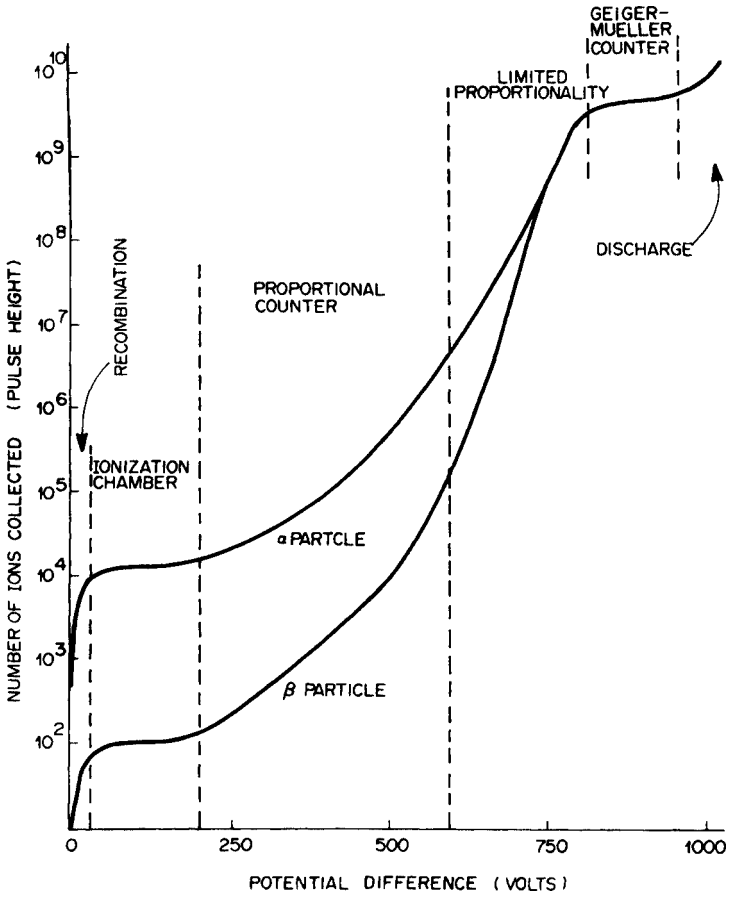

Fig. 10.4 Regions of operation of gas-filled cylindrical ionization chamber operated in pulse mode.

to allow recombination. As the potential difference is increased, the size of the pulse increases and then levels off over the plateau region, typically up to ~200 V, as shown in Fig. 10.4. When the potential difference is raised to a few hundred volts, the field strength near the anode increases to the point where electrons produced by the alpha particle and its secondary electrons acquire enough energy there to ionize additional gas atoms. Gas multiplication then occurs, and the number of ions collected in the pulse is proportional to the original number produced by the alpha particle and its secondaries. The tube operates as a proportional counter up to potential differences of ~700 V and can be used to measure the energy spectrum of individual alpha particles stopping in the gas. Gas multiplication factors of $\sim 10^4$ are typical.

When the potential difference is further increased the tube operates with limited proportionality, and then, at still higher voltage, enters the Geiger–Mueller (GM) region. In the latter mode, the field near the anode is so strong that any initial ioniza-

tion of the gas results in a pulse, the size being independent of the number of initial ion pairs. With still further increase of the voltage, the field eventually becomes so strong that it ionizes gas atoms directly and the tube continually discharges.

Compared with an alpha particle, the pulse-height curve for a beta particle is similar, but lower, as Fig. 10.4 shows. The two curves merge in the GM region.

Gas-Filled Detectors

Most ionization chambers for radiation monitoring are air-filled and unsealed, although sealed types that employ air or other gases are common. Used principally to monitor beta, gamma, and X radiation, their sensitivity depends on the volume and pressure of the gas and on the associated electronic readout components. The chamber walls are usually air equivalent or tissue equivalent in terms of the secondary-electron spectra they produce in response to the radiation.

Ionization chambers are available both as active and as passive detectors. An active detector, such as that illustrated by Fig. 10.1, gives an immediate reading in a radiation field through direct processing of the ionization current in an external circuit coupled to the chamber. Examples of this type of device include the free-air ionization chamber (Section 12.3) and the traditionally popular cutie pie (Fig. 10.5), a portable beta–gamma survey rate meter still in use today.

Passive pocket ionization chambers were used a great deal in the past. Basically a plastic condenser of known capacitance C, the unit is given a charge $Q = CV$ at a fixed potential difference V before use. Exposure to radiation produces ions in the chamber volume. These partially neutralize the charge on the chamber and

Fig. 10.5 Portable ionization-chamber survey meter (cutie pie). (Courtesy Victoreen, Inc.)

cause a voltage drop, ΔV. The amount of lost charge ΔQ, which depends on the energy absorbed, is directly proportional to the measured voltage change: $\Delta Q = C\Delta V$. Calibrated self-reading pocket ionization chambers, like that in Fig. 10.6, are still in use.

Proportional counters can be used to detect different kinds of radiation and, under suitable conditions, to measure radiation dose (Chapter 12). A variety of gases, pressures, and tube configurations are employed, depending on the intended purposes. The instrument shown in Fig. 10.7 uses a sealed gas proportional-counter

Fig. 10.6 (a) Direct-reading, condenser-type pocket ionization chamber. Amount of exposure to X and gamma radiation can be read on calibrated scale through eyepiece. (b) Charger uses standard D battery. (Courtesy Arrow-Tech, Inc.)

Fig. 10.7 Proportional-counter monitor for measuring dose and dose rate. See text. (Courtesy Berthold Technologies USA, LLC.)

probe to measure dose and dose rate. It can serve as a portable or stationary monitor. Different probes can be attached for different radiations (alpha, beta, gamma, and neutrons) and for different purposes, such as general surveys, surface contamination monitoring, or air monitoring. The basic control module, which contains extensive software, identifies the attached probe and automatically adjusts for it. Proportional-counter tubes may be either of a sealed or gas-flow type. As illustrated schematically in Fig. 10.8, the latter type of "windowless" counter is useful for counting alpha and soft beta particles, because the sample is in direct contact with the counter gas. Figure 10.9 displays such a system that monitors tritium activity concentration in air. The unit on the left regulates the incoming blend of the counter gas (methane or P-10, a mixture of 90% argon and 10% methane) with air, and also houses the detector and associated electronics. The unit on the right analyzes and displays the data. Single pulses of tritium beta particles (maximum energy 18.6 keV) are differentiated from other events by pulse-shape discrimination.

Pulse-height discrimination with proportional counters affords an easy means for detecting one kind of radiation in the presence of another. For example, to count a combined alpha–beta source with an arrangement like that in Fig. 10.8(a) or (b), one sets the discriminator level so that only pulses above a certain size are reg-

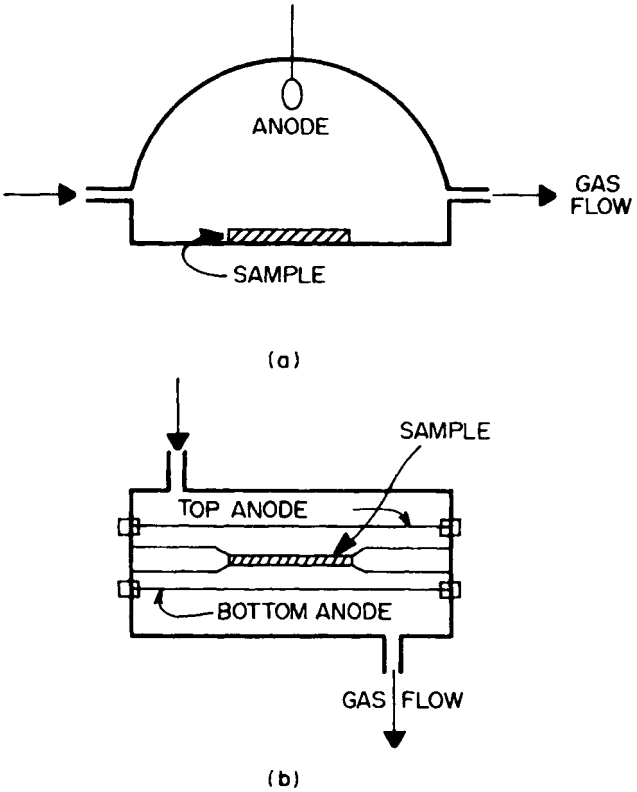

Fig. 10.8 Diagram of (a) 2π and (b) 4π gas-flow proportional counters.

istered. One then measures the count rate at different operating voltages of the tube, leaving the discriminator level set. The resulting count rate from the alpha–beta source will have the general characteristics shown in Fig. 10.10. At low voltages, only the most energetic alpha particles will produce pulses large enough to be counted. Increasing the potential difference causes the count rate to reach a plateau when essentially all of the alpha particles are being counted. With a further increase in voltage, increased gas multiplication enables pulses from the beta particles to surpass the discriminator level and be counted. At still higher voltages, a steeper combined alpha–beta plateau is reached. The use of proportional counters for neutron measurements is described in Section 10.7. Gamma-ray discrimination

Fig. 10.9 Gas-flow proportional counter for monitoring tritium activity concentration in air. See text. (Courtesy Berthold Technologies USA, LLC.)

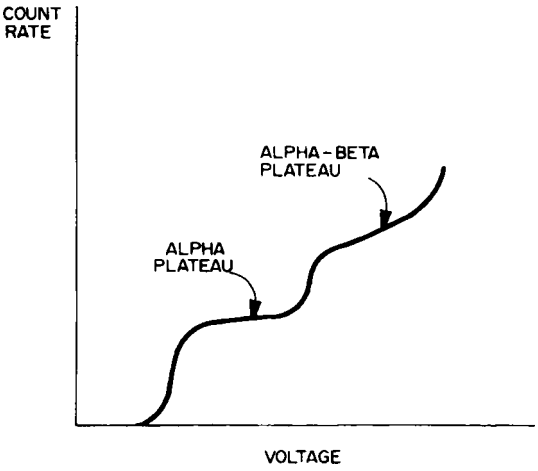

Fig. 10.10 Count rate vs. operating voltage for a proportional counter used with discriminator for counting mixed alpha–beta sources.

Fig. 10.11 Portable survey and count-rate meter with optional GM pancake probe. See text. (Courtesy Fluke Biomedical.)

is used to advantage in monitoring for neutrons in mixed gamma-neutron fields. The charged recoil nuclei from which the neutrons scatter generally produce large pulses compared to those from the Compton electrons and photoelectrons produced by the photons.

Geiger–Mueller counters are very convenient and reliable radiation monitors, providing both visual and audible responses. They usually come equipped with a removable shield that covers a thin window to enable the detection of beta and alpha particles in addition to gamma rays. Readout can be, e.g., in counts per minute or in $\mathrm{mR\,h^{-1}}$ with $^{137}\mathrm{Cs}$ calibration. With the latter, special energy compensation of the probe is needed to flatten the energy response for low-energy photons. Figure 10.11 shows an example of a counter with a pancake GM probe. The instrument is also compatible with other kinds of probes, and can be used to detect alpha, beta, gamma, and neutron radiation. Examples of various GM and scintillation (Section 10.3) probes employed in a variety of applications are shown in Fig. 10.12.

Ideally, after the primary discharge in a GM tube, the positive ions from the counter gas drift to the cathode wall, where they are neutralized. Because of the high potential difference, however, some positive ions can strike the cathode with sufficient energy to release secondary electrons. Since these electrons can initiate another discharge, leading to multiple pulses, some means of quenching the discharge must be used. By one method, called external quenching, a large resistance between the anode and high-voltage supply reduces the potential difference after each pulse. This method has the disadvantage of making the tube slow ($\sim 10^{-3}$ s) in returning to its original voltage. Internal quenching of a GM tube by addition of an appropriate gas is more common. The quenching gas is chosen with a lower ionization potential and a more complex molecular structure than the counter gas. When a positive ion of the counter gas collides with a molecule of the quench-

Fig. 10.12 Examples of Geiger–Mueller and scintillation probes with specifications. (Courtesy Fluke Biomedical.)

ing gas, the latter, because of its lower ionization potential, can transfer an electron to the counter gas, thereby neutralizing it. Positive ions of the quenching gas, reaching the cathode wall, spend their energy in dissociating rather than producing secondary electrons. A number of organic molecules (e.g., ethyl alcohol) are suitable for internal quenching. Since the molecules are consumed by the dissociation process, organically quenched GM tubes have limited lifetimes ($\sim 10^9$ counts). Alternatively, the halogens chlorine and bromine are used for quenching. Although they dissociate, they later recombine. Halogen-quenched GM tubes are often preferred for extended use, although other factors limit their lifetimes.

10.2 Ionization in Semiconductors

Band Theory of Solids

Section 2.9 briefly described crystalline solids and the origin of the band structure of their electronic energy levels. In addition to the forces that act on an electron to produce the discrete bound states in an isolated atom, neighboring atoms in the condensed phase can also affect its behavior. The influence is greatest on the motion of the most loosely bound, valence electrons in the atoms and least on the more tightly-bound, inner-shell electrons. As depicted schematically in Fig. 2.7, with many atoms present, coalescing of the discrete states into the two bands of allowed energies with a forbidden gap between them depends on the size of R_0, the orderly spacing of atoms in the crystal. The figure indicates that bands are not formed if R_0 is very large. By the same token, the bands would overlap into a single continuum with no forbidden gap if R_0 is small.

While the study of crystals is a complex subject, some insight into their electrical properties can be gained by pursuing these simple physical concepts. With isolated bands present, the upper hatched area on the far right in Fig. 2.7 is called the *conduction band*, and the lower hatched area, the *valence band*. Electrically, solids can be classified as *insulators, semiconductors,* or *conductors*. The distinction is manifest in the mobility of electrons in response to an electric field applied to the solid. This response, in turn, is intimately connected with the particular atomic/molecular crystal structure and resultant band gap. The three classifications are represented in Fig. 10.13. Like most ionic solids (Section 2.9), NaCl, for example, is an insulator. The pairing of the univalent sodium and chlorine atoms completely fills the valence band, leaving no vacancies into which electrons are free to move. In principle, thermal agitation is possible and could provide sufficient energy to promote some valence electrons into the unoccupied conduction band, where they would be mobile. However, the probability for this random occurrence is exceedingly small,

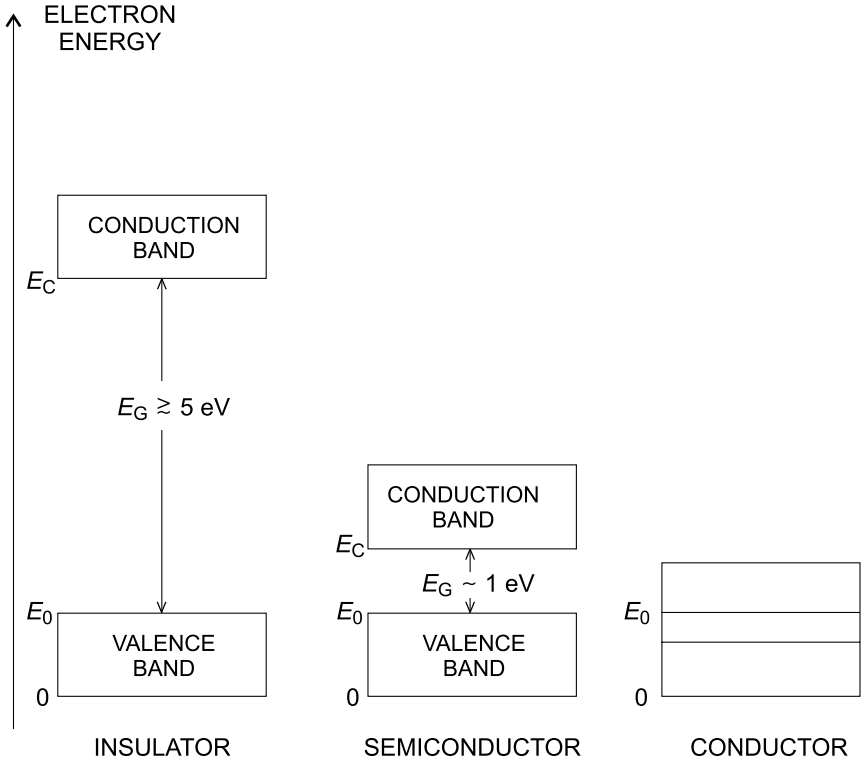

Fig. 10.13 Band structure of insulators, semiconductors, and conductors. Starting from zero at the bottom of the valence band, the vertical scale shows schematically the energies spanned by the valence and conduction bands and the forbidden gap. The energy at the top of the valence band is denoted by E_0. The energy at the bottom of the conduction band is $E_C = E_0 + E_G$, where E_G is the size of the band gap.

because the excitation energy required to span the forbidden gap is of the order of 8.5 eV. Generally, when the gap is greater than about 5 eV, the material is an insulator. While the details are different, a similar situation describes the covalent solids. The width of the band gap in carbon is 5.4 eV, making it an insulator. In silicon the gap is 1.14 eV and in germanium, 0.67 eV. At absolute zero temperature the valence bands in these two metals are completely filled and the conduction band is empty. They are insulators. At room temperatures ($kT \sim 0.025$ eV), a small fraction of their electrons are thermally excited into the conduction band, giving them some conductivity. Covalent solids having an energy gap $\sim$1 eV are called intrinsic semiconductors. In conductors, the valence and conduction bands merge, as indicated in Fig. 10.13, providing mobility to the valence electrons. Sodium, with its single atomic ground-state 3s electron is a conductor in the solid phase.

We focus now on semiconductors and the properties that underlie their importance for radiation detection and measurement. One can treat conduction electrons in the material as a system of free, identical spin-$\frac{1}{2}$ particles (Sections 2.5, 2.6). They can exchange energy with one another, but otherwise act independently, like molecules in an ideal gas, except that they also obey the Pauli exclusion principle. Under these conditions, it is shown in statistical mechanics that the average number $N(E)$ of electrons per quantum state of energy E is given by the Fermi distribution,

$$N(E) = \frac{1}{e^{(E-E_F)/kT} + 1}. \tag{10.6}$$

Here k is the Boltzmann constant, T is the absolute temperature, and E_F is called the *Fermi energy*. At any given time, each quantum state in the system is either empty or occupied by a single electron. The value of $N(E)$ is the probability that a state with energy E is occupied. To help understand the significance of the Fermi energy, we consider the distribution at the temperature of absolute zero, $T = 0$. For states with energies $E > E_F$ above the Fermi energy, the exponential term in the denominator of (10.6) in infinite; and so $N(E) = 0$. For states with energies below E_F, the exponential term is zero; and so $N(E) = 1$. Thus, all states in the system below E_F are singly occupied, while all above E_F are empty. This configuration has the lowest energy possible, as expected at absolute zero. At temperatures $T > 0$, the Fermi energy is defined as that energy for which the average, or probable, number of electrons is $\frac{1}{2}$.

It is instructive to diagram the relative number of free electrons as a function of energy in various types of solids at different temperatures. Figure 10.14(a) shows the energy distribution of electrons in the conduction band of a conductor at a temperature above absolute zero ($T > 0$). Electrons occupy states with a thermal distribution of energies above E_C. The lower energy levels are filled, but unoccupied states are available for conduction near the top of the band. A diagram for the same conductor at $T = 0$ is shown in Fig. 10.14(b). All levels with $E < E_F$ are occupied and all with $E > E_F$ are unoccupied.

Figure 10.15(a) shows the electron energy distribution in an insulator with $T > 0$. The valence band is full and the forbidden-gap energy E_G ($\sim$5 eV) is so wide that the electrons cannot reach the conduction band at ordinary temperatures. Fig-

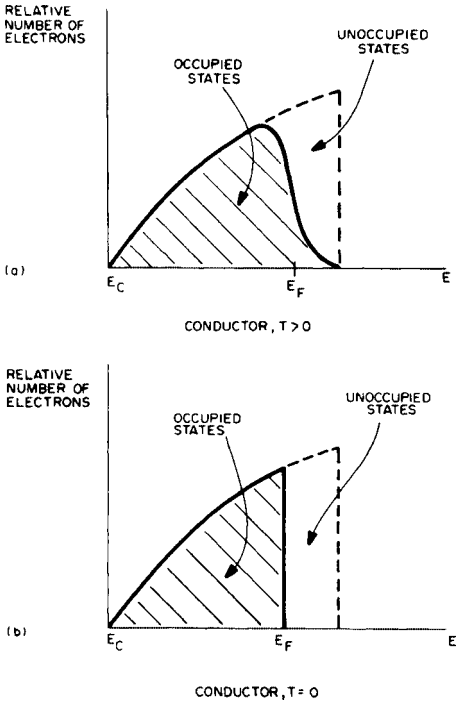

Fig. 10.14 Relative number of electrons in the conduction band of a conductor at absolute temperatures (a) $T > 0$ and (b) $T = 0$.

ure 10.15(b) shows a semiconductor in which $E_G \sim 1$ eV is considerably narrower than in the insulator. The tail of the thermal distribution [Eq. (10.6)] permits a relatively small number of electrons to have energies in the conduction band. In this case, the number of occupied states in the conduction band is equal to the number of vacant states in the valence band and E_F lies midway in the forbidden gap at an energy $E_0 + E_G/2$. At room temperature, the density of electrons in the conduction band is 1.5×10^{10} cm^{-3} in Si and 2.4×10^{13} cm^{-3} in Ge.

Semiconductors

Figure 10.16 schematically represents the occupation of energy states for the semiconductor from Fig. 10.15(b) with $T > 0$. The relatively small number of electrons in the conduction band are denoted with minus signs and the equal number of positive ions they leave in the valence band with plus signs. The combination of two charges is called an electron–hole pair, roughly analogous to an ion pair in a gas. Under the influence of an applied electric field, electrons in the conduction band will move. In addition, electrons in the valence band move to fill the holes, leaving other holes in their place, which in turn are filled by other electrons, and so on. This, in effect, causes the holes to migrate in the direction opposite to that of the electrons. The motions of both the conduction-band electrons and the valence-band

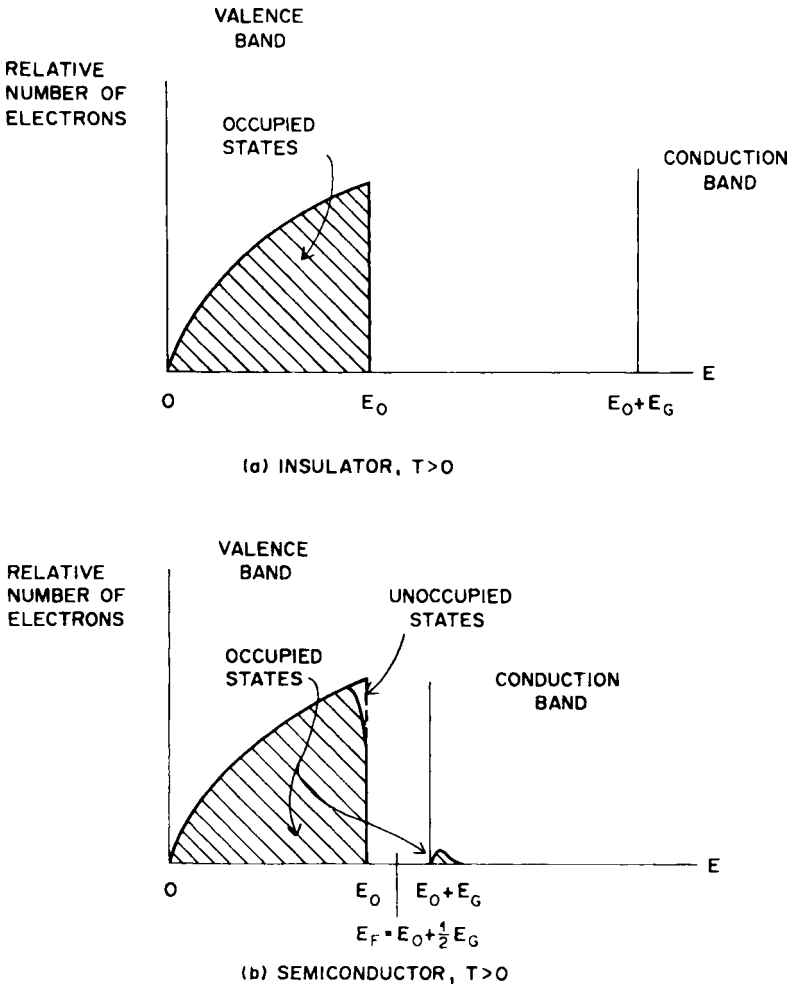

Fig. 10.15 Relative number of electrons in valence and conduction bands of (a) an insulator and (b) a semiconductor with $T > 0$.

holes contribute to the observed conductivity. The diagram in Fig. 10.16 represents an intrinsic (pure) semiconductor. Its inherent conductivity at room temperature is restricted by the small number of electron–hole pairs, which, in turn, is limited by the size of the gap compared with kT.

The conductivity of a semiconductor can be greatly enhanced by doping the crystal with atoms from a neighboring group in the periodic system. As an example, we consider the addition of a small amount of arsenic to germanium.[1)] When a crystal is formed from the molten mixture, the arsenic impurity occupies a substitutional

1 The reader is referred to the Periodic Table at the back of the book.

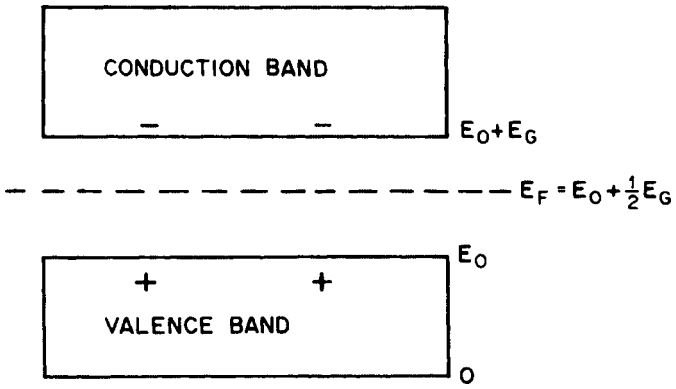

Fig. 10.16 Occupation of energy states in an intrinsic semiconductor at room temperature. A relatively small number of electrons (–) are thermally excited into the conduction band, leaving an equal number of holes (+) in the valence band. The Fermi energy E_F lies at the middle of the forbidden gap.

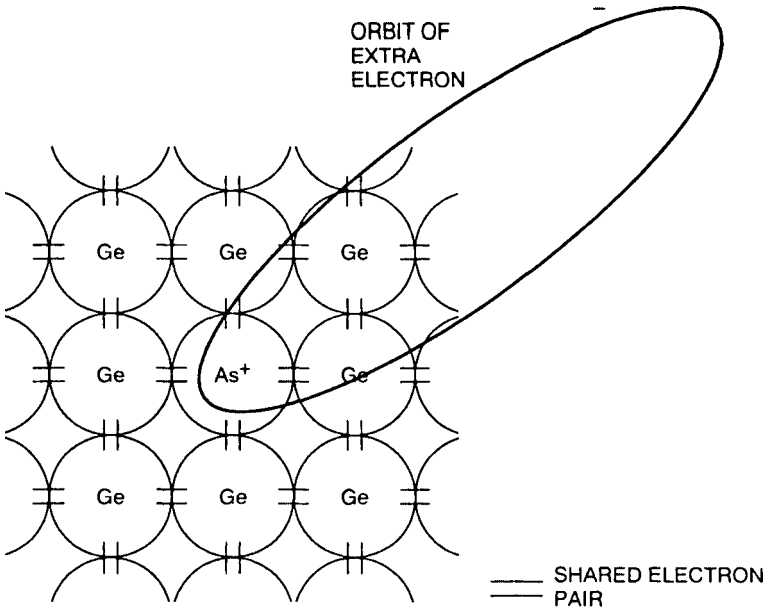

Fig. 10.17 Addition of a small quantity of pentavalent As to Ge crystal lattice provides very loosely bound "extra" electrons that have a high probability of being thermally excited into the conduction band at room temperatures. Arsenic is called a donor impurity and the resulting semiconductor, n-type.

position in the germanium lattice, as indicated schematically in Fig. 10.17. (The As atom has a radius of 1.39 Å compared with 1.37 Å for Ge.) Since As has five valence electrons, there is one electron left over after all of the eight covalent bonds

have been formed with the neighboring Ge atoms. In Fig. 10.17, two short straight lines are used to represent a pair of electrons shared covalently by neighboring atoms and the loop represents, very schematically, the orbit of the extra electron contributed by As^+, which is in the crystal lattice. There is no state for the extra electron to occupy in the filled valence band. Since it is only very loosely bound to the As^+ ion (its orbit can extend over several tens of atomic diameters), this electron has a high probability of being thermally excited into the conduction band at room temperature. The conductivity of the doped semiconductor is thus greatly increased over its value as an intrinsic semiconductor. The amount of increase can be controlled by regulating the amount of arsenic added, which can be as little as a few parts per million. An impurity such as As that contributes extra electrons is called a donor and the resulting semiconductor is called n-type (negative).

Since little energy is needed to excite the extra electrons of an n-type semiconductor into the conduction band, the energy levels of the donor impurity atoms must lie in the forbidden gap just below the bottom of the conduction band. The energy-level diagram for Ge doped with As is shown in Fig. 10.18. The donor states are found to lie 0.013 eV below the bottom of the conduction band, as compared with the total gap energy, $E_G = 0.67$ eV, for Ge. At absolute zero all of the donor states are occupied and no electrons are in the conduction band. The Fermi energy lies between the donor levels and the bottom of the conduction band. As T is increased, thermally excited electrons enter the conduction band from the donor states, greatly increasing the conductivity. Antimony can also be used as a donor impurity in Ge or Si to make an n-type semiconductor.

Another type of semiconductor is formed when Ge or Si is doped with gallium or indium, which occur in the adjacent column to their left in the periodic system.

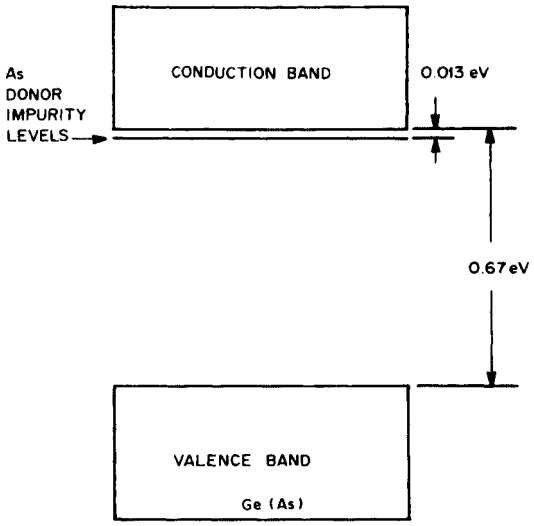

Fig. 10.18 Energy-level diagram for Ge crystal containing As donor atoms (n-type semiconductor).

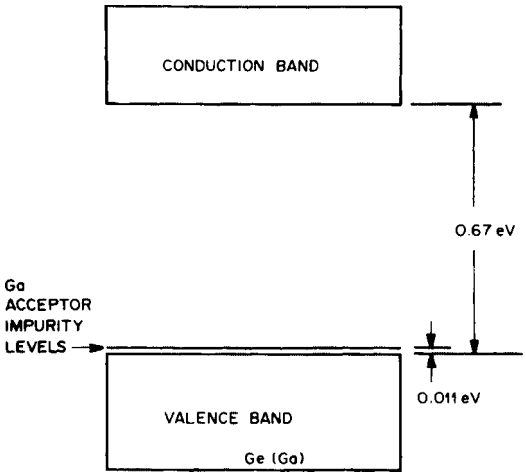

Fig. 10.19 Energy-level diagram for Ge crystal containing Ga acceptor atoms (p-type semiconductor).

In this case, the valence shell of the interposed impurity atom has one less electron than the number needed to form the regular covalent crystal. Thus, the doped crystal contains positively charged "holes," which can accept electrons. The dopant is then called an acceptor impurity and the resulting semiconductor, p-type (positive). Holes in the valence band move like positive charges as electrons from neighboring atoms fill them. Because of the ease with which valence-band electrons can move and leave holes with the impurity present, the effect of the acceptor impurity is to introduce electron energy levels in the forbidden gap slightly above the top of the valence band. Figure 10.19 shows the energy-level diagram for a p-type Ge semiconductor with Ga acceptor atoms added. The action of the p-type semiconductor is analogous to that of the n-type. At absolute zero all of the electrons are in the valence band, the Fermi energy lying just above. When $T > 0$, thermally excited electrons occupy acceptor-level states, giving enhanced conductivity to the doped crystal.

Semiconductor Junctions

The usefulness of semiconductors as electronic circuit elements and for radiation measurements stems from the special properties created at a diode junction where n- and p-type semiconductors are brought into good thermodynamic contact. Figure 10.20 shows an electron energy-level diagram for an n–p junction. The two semiconductor types in contact form a single system with its own characteristic Fermi energy E_F. Because E_F lies just below the conduction band in the isolated n region and just above the valence band in the isolated p region, the bands must become deformed over the junction region, as shown in the figure. When the n- and p-type semiconductors are initially brought into contact, electrons flow from the donor impurity levels on the n side over to the lower-energy acceptor sites on

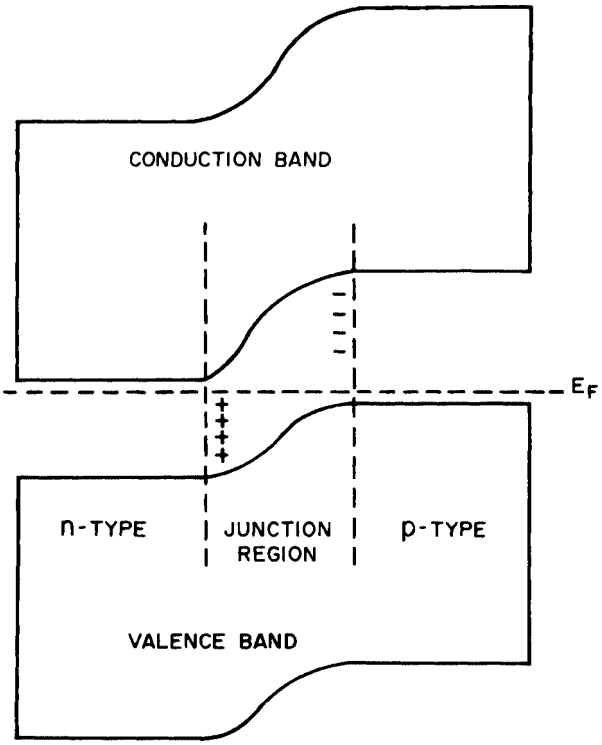

Fig. 10.20 Energy-level diagram for n–p junction.

the p side. This process accumulates negative charge on the p side of the junction region and leaves behind immobile positive charges on the n side in the form of ionized donor impurity atoms. The net effect at equilibrium is the separation of charge across the junction region (as indicated by the + and – symbols in Fig. 10.20) and the maintenance of the deformed bands.

Even with thermal equilibrium, electrons move both ways through the junction region. With reference to Fig. 10.20, thermal agitation will cause some electrons to get randomly promoted into the conduction band in the p region, at the same time leaving holes in the valence band. A promoted electron can then travel freely to the junction region, where it will be drawn into the n region. This process gives rise to a spontaneous *thermal current* of electrons in the direction from the p to the n side of the junction. Also, some conduction-band electrons in the n region randomly receive enough energy to be able to move into the p region. There an electron can combine with a vacated hole in the valence band. This process provides a *recombination current* of electrons from the n to the p side. It balances the thermal current, so that no net charge flows through the device. Holes in the valence band appear to migrate by being successively filled by neighboring electrons, thus acting like positive charge carriers. Silicon devices (1.14 eV band gap) operate at room temperatures. The smaller gap of germanium (0.67 eV) necessitates operation at low temperatures (e.g., 77 K, liquid nitrogen) to suppress thermal noise.

The junction region over which the charge imbalance occurs is also called the depletion region, because any mobile charges initially there moved out when the two sides were joined. The depletion region acts, therefore, like a high-resistivity parallel-plate ionization chamber, making it feasible to use it for radiation detection. Ion pairs produced there will migrate out, their motion giving rise to an electrical signal. The performance of such a device is greatly improved by using a bias voltage to alleviate recombination and noise problems. The biased junction becomes a good rectifier, as described next.

Consider the n–p junction device in Fig. 10.21(a) with the negative side of an external bias voltage V applied to the n side. When compared with Fig. 10.20, it is seen that the applied voltage in this direction lowers the potential difference across the junction region and causes a relatively large current I to flow in the circuit. Bias in this direction is called forward, and a typical current–voltage curve is shown at the right in Fig. 10.21(a). One obtains a relatively large current with a small bias voltage. When a reverse bias is applied in Fig. 10.21(b), comparison with Fig. 10.20 shows that the potential difference across the junction region increases. Therefore, a much smaller current flows—and in the opposite direction—under reverse bias, as illustrated on the right in Fig. 10.21(b). Note the vastly different voltage and current scales on the two curves in the figure. Such n–p junction devices are rectifiers, passing current readily in one direction but not the other.

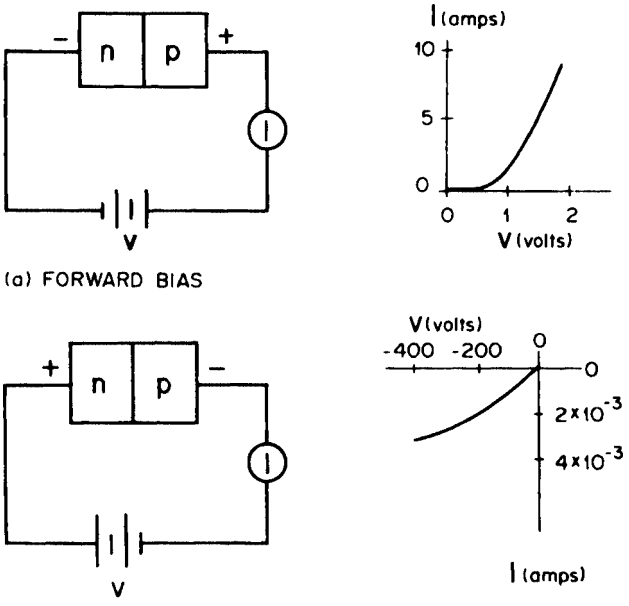

Fig. 10.21 (a) Forward- and (b) reverse-biased n–p junctions and typical curves of current vs. voltage. Note the very different scales used for the two curves. Such an n–p junction is a good rectifier.

Radiation Measuring Devices

The reverse-biased n–p junction constitutes an attractive radiation detector. The depletion region, which is the active volume, has high resistivity, and ions produced there by radiation can be collected swiftly and efficiently. It can serve as a rate meter or to analyze pulses. The number of electron–hole pairs produced in a pulse is proportional to the energy absorbed in the active volume, and so the junction can be used as a spectrometer. The "*W* values" for Si and Ge are, respectively, 3.6 eV and 3.0 eV per electron–hole pair, as compared with the corresponding figure of ~30 eV per ion pair in gases. Statistically, the relatively large number of charge carriers produced per unit energy absorbed in semiconductors endows them with much better energy resolution than other detectors. Unique among detectors is the fact that the physical size of the depletion region can be varied by changing the bias voltage. For measuring alpha and beta radiation, junctions are fabricated with a very thin surface barrier between the outside of the device and the depletion region. Several examples of semiconductor radiation instruments will be briefly described.

Electronic dosimeters have advanced rapidly in recent years. They are in widespread use, particularly in nuclear power-plant, home-security, and military applications. Figure 10.22 shows a silicon diode personal electronic dosimeter for photons in the energy range 50 keV to 6 MeV. Other models in the series measure photons down to 20 keV and beta radiation. The unit operates as both a passive and an active dosimeter. It has adjustable dose and dose-rate warning and alarm levels. It can be used either in an autonomous or in a satellite mode, with remote computer interfacing with exposure-records management software. The device performs regular internal operating checks and reports dose increments, date, and time at specified intervals. A microprocessor counts pulses, converts them to dose, and calculates dose rate.

High-purity germanium (HPGe) detectors are available for a wide variety of tasks (Fig. 10.23). The crystals are housed in a vacuum-tight cryostat unit, which typically contains the preamplifier in a cylindrical package. Depending on the intended application, germanium detectors come in a number of different planar and coaxial configurations.

A light-weight, rugged, portable multichannel analyzer for gamma spectra is shown in Fig. 10.24. It is controlled from a key pad connected through an interface module to the HPGe detector. The unit has 16k channels and gives a live display of data being acquired. It holds 23 spectra in its internal memory. Nuclide ID and activity calculations are performed by using stored calibration information. The instrument can also interface with a computer to utilize other software applications.

CZT is the name given to *cadmium zinc telluride* semiconductors, which operate at normal temperatures. The relatively high-density crystal is advantageous for stopping secondary electrons. The resolution is intermediate between Ge and Si. With its high sensitivity for gamma detection, CTZ applications include homeland security, waste effluent monitoring, and first-responder technology. Detectors, such as the one shown in Fig. 10.25, are small, rugged, programmable, and operate with very low energy consumption.

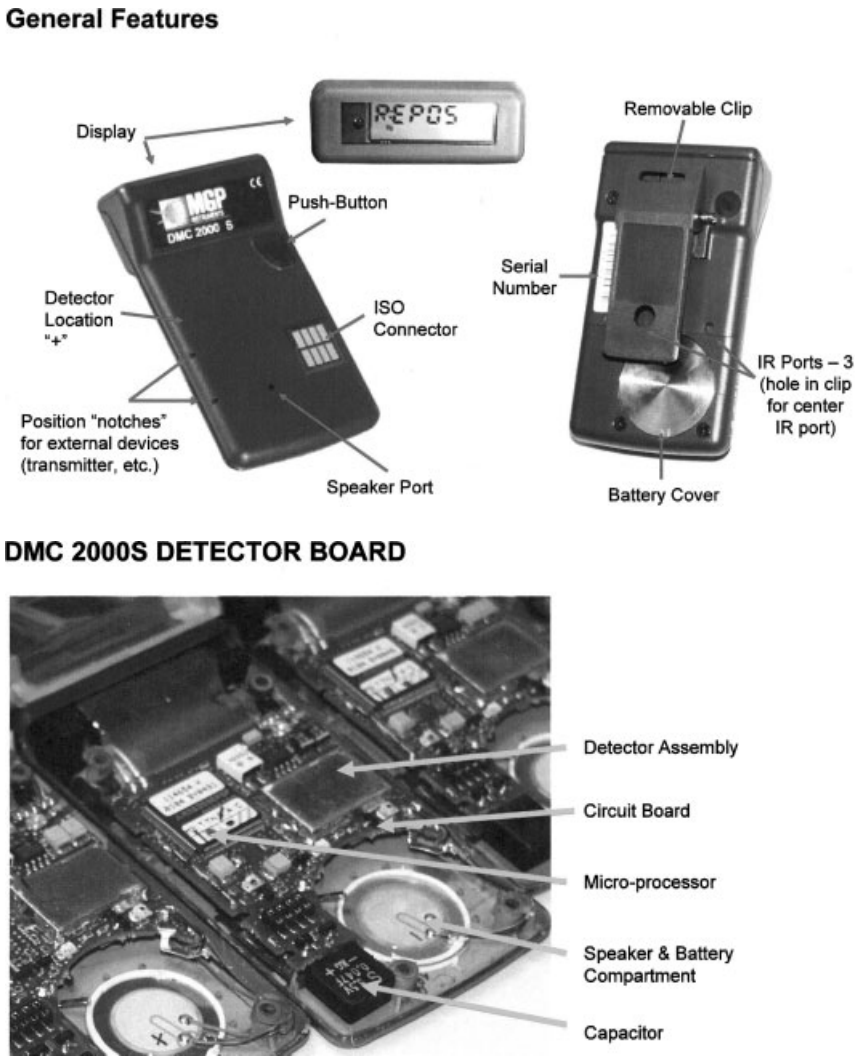

Fig. 10.22 Silicon diode electronic dosimeter. See text for description. (Courtesy MGP Instruments, Inc.)

The sensitive lung counter in Fig. 10.26 employs three coaxial HPGe crystal detectors. It is specially designed to measure the relatively low-energy (15 keV–400 keV) gamma and X rays emitted by uranium and other actinides in the lung (e.g., ^{241}Am, ^{239}Pu, ^{238}Pu, ^{237}Np). If there is insoluable material in the organ, it is not amenable to bioassay monitoring. External measurements to identify the weak photons in the presence of background entail considerable technical challenges. The counter is calibrated with torso phantoms, employing a series of chest-wall plates, like the one shown in the figure. Calibration phantoms, having differing thicknesses of overlay and fat-to-muscle ratios are used to better represent a wide

Fig. 10.23 Examples of HPGe detectors. (Courtesy Canberra, Inc.)

Fig. 10.24 Portable HPGe multichannel analyzer. (Image provided courtesy of ORTEC, a brand of Advanced Measurement Technology, AMETEK.)

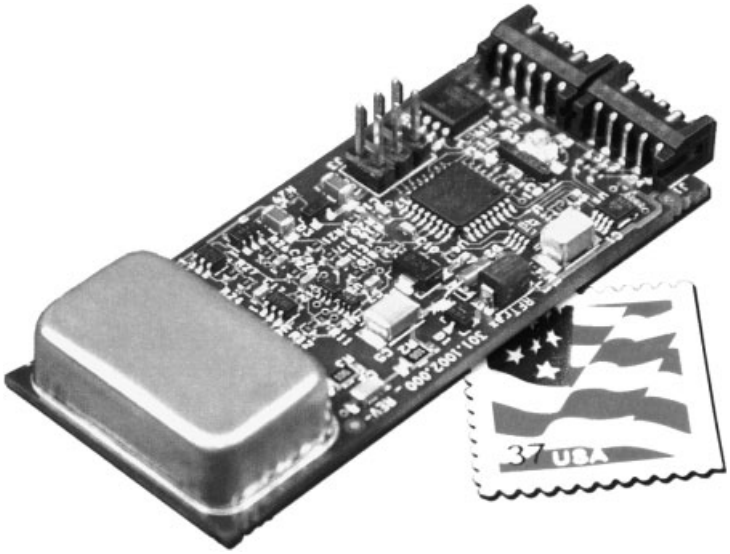

Fig. 10.25 Cadmium zinc telluride (CZT) crystal detector. (Courtesy RFTrax, Inc.)

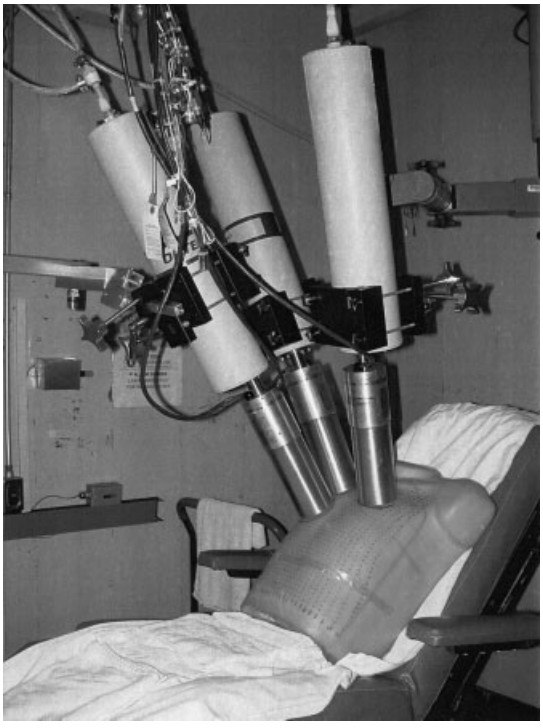

Fig. 10.26 ORNL lung counter with calibration torso. See text. (Courtesy Robert L. Coleman, Oak Ridge National Laboratory, managed by UT-Battelle, LLC, for the U.S. Department of Energy.)

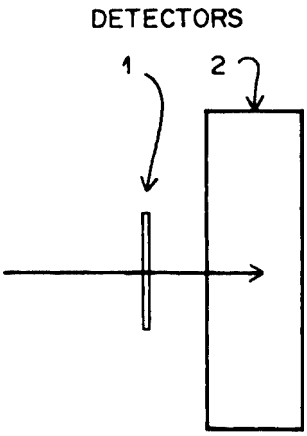

Fig. 10.27 Particle identifier.

range of male and female subjects. Ultrasound measurements are used to correlate calibration parameters with the height and weight of persons being measured. For reduced background, the facility is shielded by 14-inch thick irreplaceable steel from pre-World-War II battleships, free of radioisotopes of cobalt, cesium, and other nuclides of the atomic age.

The *particle identifier* utilizes two detectors in the configuration shown in Fig. 10.27. A heavy particle passes through a thin detector (1) and is stopped in a thick detector (2). The pulse height from 1 is proportional to the stopping power, $-\mathrm{d}E/\mathrm{d}x$, and that from 2 is proportional to the kinetic energy, $E = Mv^2/2$, with which the particle enters it, where M is the particle's mass and v is its velocity. The signals from 1 and 2 can be combined electronically in coincidence to form the product $E(-\mathrm{d}E/\mathrm{d}x)$. Since the ln term in the stopping-power formula [Eq. (5.23)] varies slowly with the particle energy E, it follows that

$$E\left(-\frac{\mathrm{d}E}{\mathrm{d}x}\right) = kz^2M, \tag{10.7}$$

approximately, where z is the particle's charge and k is a constant of proportionality. The quantity z^2M, which is thus determined by the measurement, is characteristic of a particular heavy particle, which can then be identified.

10.3 Scintillation

General

Scintillation was the first method used to detect ionizing radiation (Roentgen having observed the fluorescence of a screen when he discovered X rays). When radiation loses energy in a luminescent material, called a scintillator or phosphor, it causes electronic transitions to excited states in the material. The excited states

decay by emitting photons, which can be observed and related quantitatively to the action of the radiation. If the decay of the excited state is rapid (10^{-8} or 10^{-9} s), the process is called fluorescence; if it is slower, the process is called phosphorescence.

Scintillators employed for radiation detection are usually surrounded by reflecting surfaces to trap as much light as possible. The light is fed into a photomultiplier tube for generation of an electrical signal. There a photosensitive cathode converts a fraction of the photons into photoelectrons, which are accelerated through an electric field toward another electrode, called a dynode. In striking the dynode, each electron ejects a number of secondary electrons, giving rise to electron multiplication. These secondary electrons are then accelerated through a number of additional dynode stages (e.g., 10), achieving electron multiplication in the range 10^7–10^{10}. The magnitude of the final signal is proportional to the scintillator light output, which, under the right conditions, is proportional to the energy loss that produced the scintillation.

Since materials emit and absorb photons of the same wavelength, impurities are usually added to scintillators to trap energy at levels such that the wavelength of the emitted light will not fall into a self-absorption region. Furthermore, because many substances, especially organic compounds, emit fluorescent radiation in the ultraviolet range, impurities are also added as wavelength shifters. These lead to the emission of photons of visible light, for which glass is transparent and for which the most sensitive photomultiplier tubes are available.

Good scintillator materials should have a number of characteristics. They should efficiently convert the energy deposited by a charged particle or photon into detectable light. The efficiency of a scintillator is defined as the fraction of the energy deposited that is converted into visible light. The highest efficiency, about 13%, is obtained with sodium iodide. A good scintillator should also have a linear energy response; that is, the constant of proportionality between the light yield and the energy deposited should be independent of the particle or photon energy. The luminescence should be rapid, so that pulses are generated quickly and high count rates can be resolved. The scintillator should also be transparent to its own emitted light. Finally, it should have good optical quality for coupling to a light pipe or photomultiplier tube. The choice of a particular scintillation detector represents a balancing of these factors for a given application.

Two types of scintillators, organic and inorganic, are used in radiation detection. The luminescence mechanism is different in the two.

Organic Scintillators

Fluorescence in organic materials results from transitions in individual molecules. Incident radiation causes electronic excitations of molecules into discrete states, from which they decay by photon emission. Since the process is molecular, the same fluorescence can occur with the organic scintillator in the solid, liquid, or vapor state. Fluorescence in an inorganic scintillator, on the other hand, depends on the existence of a regular crystalline lattice, as described in the next section.

Organic scintillators are available in a variety of forms. Anthracene and stilbene are the most common organic crystalline scintillators, anthracene having the highest efficiency of any organic material. Organic scintillators can be polymerized into plastics. Liquid scintillators (e.g., xylene, toluene) are often used and are practical when large volumes are required. Radioactive samples can be dissolved or suspended in them for high-efficiency counting. Liquid scintillators are especially suited for measuring soft beta rays, such as those from ^{14}C or ^{3}H. High-Z elements (e.g., lead or tin) are sometimes added to organic scintillator materials to achieve greater photoelectric conversion, but usually at the cost of decreased efficiency.

Compared with inorganic scintillators, organic materials have much faster response, but generally yield less light. Because of their low-Z constituents, there are little or no photoelectric peaks in gamma-ray pulse-height spectra without the addition of high-Z elements. Organic scintillators are generally most useful for measuring alpha and beta rays and for detecting fast neutrons through the recoil protons produced.

Inorganic Scintillators

Inorganic scintillator crystals are made with small amounts of activator impurities to increase the fluorescence efficiency and to produce photons in the visible region. As shown in Fig. 10.28, the crystal is characterized by valence and conduction bands, as described in Section 10.2. The activator provides electron energy levels in the forbidden gap of the pure crystal. When a charged particle interacts with the crystal, it promotes electrons from the valence band into the conduction band, leaving behind positively charged holes. A hole can drift to an activator site and ionize it. An electron can then drop into the ionized site and form an excited neutral impurity complex, which then decays with the emission of a visible photon. Because the photon energies are less than the width of the forbidden gap, the crystal does not absorb them.

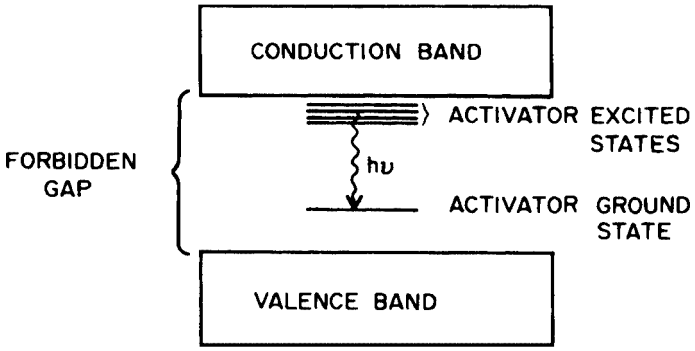

Fig. 10.28 Energy-level diagram for activated crystal scintillator. Because the energy levels of the activator complex are in the forbidden gap, the crystal is transparent at the fluorescent photon energies $h\nu$.

The alkali halides are good scintillators. In addition to its efficient light yield, sodium iodide doped with thallium [NaI(Tl)] is almost linear in its energy response. It can be machined into a variety of sizes and shapes. Disadvantages are that it is hygroscopic and somewhat fragile. NaI has become a standard scintillator material for gamma-ray spectroscopy. CsI(Na), CsI(Tl), and LiI(Eu) are examples of other inorganic scintillators. Silver-activated zinc sulfide is also commonly used. It is available only as a polycrystalline powder, from which thin films and screens can be made. The use of ZnS, therefore, is limited primarily to the detection of heavy charged particles. (Rutherford used ZnS detectors in his alpha-particle scattering experiments.) Glass scintillators are also widely used.

Two examples of scintillator probes are displayed in Fig. 10.29. In addition to the detector material, each contains a photomultiplier tube, which is reflected in its size. The unit on the left is used for gamma surveys. It has a cylindrical NaI(Tl) crystal with a height and diameter of 2.5 cm. It operates between 500 V and 1200 V. The unit on the right uses ZnS and is suitable for alpha/beta surveys. It operates in the same voltage range. The window area is approximately 100 cm^2.

Specialized scintillation devices have been designed for other specific purposes. One example is the phoswich (= phosphor sandwich) detector, which can be used to count beta particles or low-energy photons in the presence of high-energy photons. It consists of a thin NaI(Tl) crystal in front coupled to a larger scintillator of another material, often CsI(Tl), having a different fluorescence time. Signals that come from the photomultiplier tube can be distinguished electronically on the basis of the different decay times of the two phosphors to tell whether the light came only from the thin front crystal or from both crystals. In this way, the low-energy radiation can be counted in the presence of a high-energy gamma-ray background.

Figure 10.30 shows a pulse-height spectrum measured with a 4×4 in. NaI(Tl) scintillator exposed to 662-keV gamma rays from ^{137}Cs. Several features should be noted. Only those photons that lose all of their energy in the crystal contribute to the total-energy peak, also called the photopeak. These include incident photons that produce a photoelectron directly and those that undergo one or more Compton

Fig. 10.29 Examples of scintillation probes: (left) NaI(Tl) for gamma surveys; (right) ZnS for alpha/beta monitoring. (Courtesy Ludlum Instruments, Inc.)

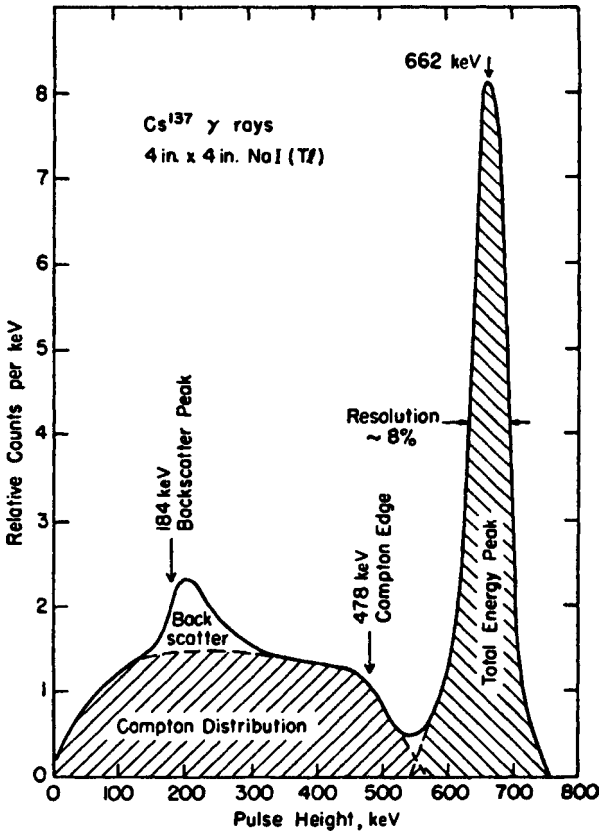

Fig. 10.30 Pulse-height spectrum measured with 4 × 4 in. NaI(Tl) scintillator exposed to 662-keV gamma rays from ^{137}Cs. The resolution is about 8% of the peak energy. The maximum Compton-electron energy is 478 keV. [Reprinted with permission from R. D. Evans, "Gamma Rays," in *American Institute of Physics Handbook*, 3d ed., p. 8-210, McGraw-Hill, New York (1972). Copyright 1972 by McGraw-Hill Book Company.]

scatterings and then produce a photoelectron. In the latter case, the light produced by the Compton recoil electrons and that produced by the final photoelectron combine to yield a single scintillation pulse around 662 keV. (The light produced by Auger electrons and characteristic X rays absorbed in the crystal is also included in the same pulse, these processes taking place rapidly.) Other photons escape from the crystal after one or more Compton scatterings, and therefore do not deposit all of their energy in producing the scintillation. These events give rise to the continuous Compton distribution at lower pulse heights, as shown in the figure. The Compton edge at 478 keV is the maximum Compton-electron recoil energy, $T_{\max}$, given by Eq. (8.20). The pulses that exceed $T_{\max}$ in magnitude come from two or more Compton recoil electrons produced by the photon before it escapes from the

crystal. The backscatter peak is caused by photons that are scattered into the scintillator from surrounding materials. The energy of a ^{137}Cs gamma ray that is scattered at 180° is $662 - T_{max} = 662 - 478 = 184$ keV. The backscattered radiation peaks at an energy slightly above this value, as shown.

The relative area under the total-energy peak and the Compton distribution in Fig. 10.30 depends on the size of the scintillator crystal. If the crystal is very large, then relatively few photons escape. Most of the pulses occur around 662 keV. If it is small, then only single interactions are likely and the Compton continuum is large. In fact, the ratio of the areas under the total-energy peak and the Compton distribution in a small detector is equal to the ratio of the photoelectric and Compton cross sections in the crystal material.

The occurrence of so-called escape peaks is accentuated when a detector is small, whether it be a scintillator or semiconductor. In NaI, for example, when a K-shell vacancy in iodine following photoelectric absorption is filled by an L-shell electron, a 28-keV characteristic X ray is emitted. The X ray will likely escape if the crystal is small, and a pulse size of $h\nu_0 - 28$ keV will be registered, where $h\nu_0$ is the energy of the incident photon. When the incident photons are monoenergetic, the pulse-height spectrum shows the escape peak, as illustrated in Fig. 10.31. The relative size of the peaks at the two energies $h\nu_0$ and $h\nu_0 - 28$ keV depends on the physical dimensions of the NaI crystal. Germanium has an X-ray escape peak 11 keV below the photopeak. Another kind of escape peak can occur in the pulse-height spectra of monoenergetic high-energy photons of energy $h\nu_0$, which produce electron–positron pairs in the detector. The positron quickly stops and annihilates with an

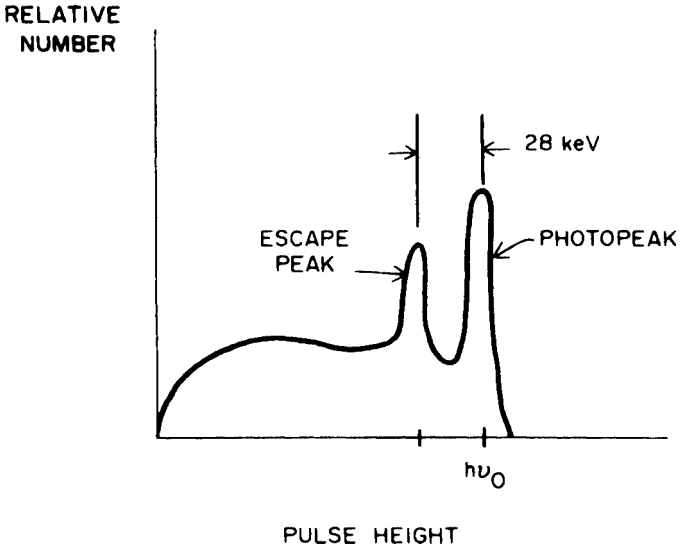

Fig. 10.31 When characteristic X rays from iodine escape from a NaI scintillator, an escape peak appears 28 keV below the photopeak.

atomic electron, producing two 0.511-MeV photons. In small detectors one or both annihilation photons can escape without interacting, leading to escape peaks at the energies $h\nu_0 - 0.511$ and $h\nu_0 - 1.022$ MeV.

An example of a portable NaI gamma analyzer for laboratory and field use is shown in Fig. 10.32. It has 512 channels and can store 30 spectra in memory. The instrument displays spectra and dose rates, as seen in the figure. Software includes peak analysis, nuclide identification search, and capability for data transfer. Adjustable alarm thresholds with an audible signal can be set.

Example

Monoenergetic 450-keV gamma rays are absorbed in a NaI(Tl) crystal having an efficiency of 12%. Seventy-five percent of the scintillation photons, which have an average energy of 2.8 eV, reach the cathode of a photomultiplier tube, which converts 20% of the incident photons into photoelectrons. Assume that variations in the pulse heights from different gamma photons are due entirely to statistical fluctuations in the number of visible photons per pulse that reach the cathode. (a) Calculate the average number of scintillation photons produced per absorbed gamma photon. (b) How many photoelectrons are produced, on the average, per gamma photon? (c) What is the average energy expended by the incident photon to produce a photoelectron from the cathode of the photomultiplier tube (the "W value")? (d) Compare this value with the average energy needed to produce an ion pair in a gas or a semiconductor.

Solution

(a) The total energy of the visible light produced with 12% efficiency is 450 keV $\times$ $0.12 = 54.0$ keV. The average number of scintillation photons is therefore 54,000/ $2.8 = 19{,}300$. (b) The average number of photons that reach the photomultiplier cathode is $0.75 \times 19{,}300 = 14{,}500$, and so the average number of photoelectrons that produce a pulse is $0.20 \times 14{,}500 = 2900$. (c) Since one 450-keV incident gamma photon produces an average of 2900 photoelectrons that initiate the signal, the "W value" for the scintillator is $450{,}000/2900 = 155$ eV/photoelectron. (d) For gases, $W \sim 30$ eV ip^{-1}; and so the average number of electrons produced by absorption of a photon would be about $450{,}000/30 = 15{,}000$. For a semiconductor, $W \sim 3$ eV ip^{-1} and the corresponding number of electrons would be 150,000. A "W value" of several hundred eV per electron produced at the photocathode is typical for scintillation detectors. Energy resolution is discussed in Section 11.11.

The energy resolution of a spectrometer depends on several factors, such as the efficiency of light or charge collection and electronic noise. Resolution is also inherently limited by random fluctuations in the number of charge carriers collected when a given amount of energy is absorbed in the detector. As the last example shows, the number of charge carriers produced in germanium is substantially larger than that in a scintillator. Therefore, as discussed in the next chapter, the *relative* fluctuation about the mean—the inherent resolution—is much better for germanium. The upper panel in the example presented in Fig. 10.33 compares pulse-height spectra measured with a NaI detector for pure ^{133}Ba and for a mixture of ^{133}Ba and ^{239}Pu. The soft Pu gamma photons, at energies marked by the arrows, are not distinguished.

(a)

(b)

Fig. 10.32 (a) Hand-held NaI gamma analyzer and dose-rate meter with (b) close-up of display. (Courtesy Berthold Technologies USA, LLC.)

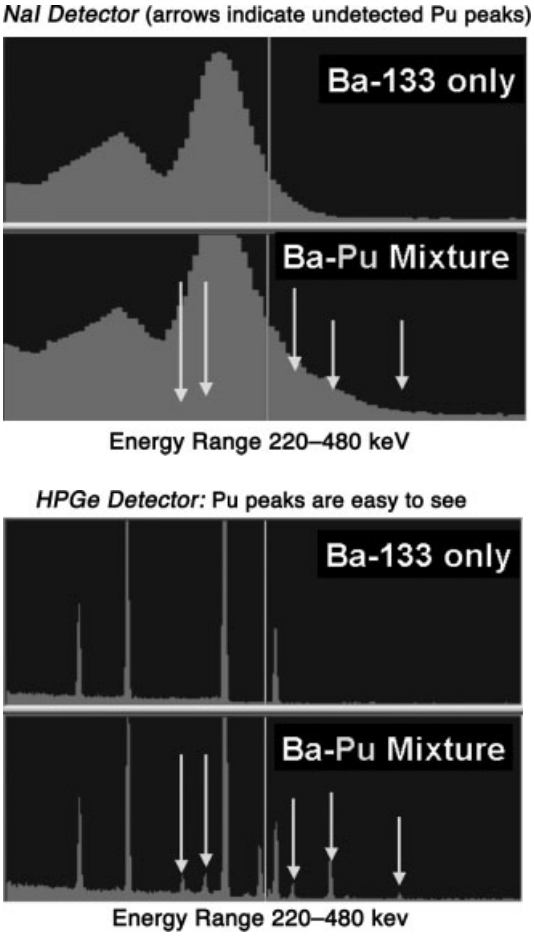

Fig. 10.33 Comparison of spectra of ^{133}Ba and ^{133}Ba-^{239}Pu mixture made with NaI and HPGe detectors. (Image provided courtesy of ORTEC, a brand of Advanced Measurement Technology, AMETEK.)

The lower panel compares the same spectra measured with HPGe. With this much greater resolution, the presence of both nuclides is unmistakable.

Research has accelerated on the development of new scintillation as well as other methods of radiation detection, driven by concerns for homeland security. Large inorganic scintillators provide the most sensitive means for general detection of gamma rays. Promising new approaches in this direction include the investigation of cerium-doped lanthanum halides, $LaCl_3 : Ce^{3+}$ and $LaBr_3 : Ce^{3+}$. Large crystals can be produced with relatively high light yield and good energy resolution. Figure 10.34 shows radiation monitors in place at a typical border crossing into the United States.

Fig. 10.34 Sensitive monitors installed at portals in passenger lanes of border crossings into the U.S. can detect small amounts of radioactive material. Alarms are sometimes triggered by naturally radioactive agricultural products, ceramic tiles, and occasionally by a passenger, recently administered radioactive thalium, technetium, or iodine by a physician. (Courtesy Joseph C. McDonald. Reprinted with permission from "Detecting Illicit Radioactive Sources," by Joseph C. McDonald, Bert M. Coursey, and Michael Carter in Physics Today, November 2004. Copyright 2004, American Institute of Physics.)

10.4 Photographic Film

Since the early days of experience with ionizing radiation, films have been used extensively for detection and measurement. (Recall from Section 1.3 how Becquerel discovered radioactivity.) Film emulsions contain small crystals of a silver halide (e.g., AgBr), suspended in a gelatine layer spread over a plastic or glass surface, wrapped in light-tight packaging. Under the action of ionizing radiation, some secondary electrons released in the emulsion become trapped in the crystalline lattice, reducing silver ions to atomic silver. Continued trapping leads to the formation of microscopic aggregates of silver atoms, which comprise the latent image. When developed, the latent images are converted into metallic silver, which appears to the eye as darkening of the film. The degree of darkening, called the optical density, increases with the amount of radiation absorbed. An optical densitometer can be used to measure light transmission through the developed film.

Badges containing X-ray film packets have been worn, clipped to the clothing, for beta–gamma personnel radiation-dose monitoring and for worker identification. As discussed below, doses from gamma and beta radiation can be inferred by comparing densitometer readings from exposed film badges with readings from a calibrated set of films given different, known doses under the same conditions. The darkening response of film to neutrons, on the other hand, is too weak to be used in this way for neutron personnel monitoring. Instead, special fine-grain, nu-

clear track emulsions are employed. The tracks of individual recoil protons that neutrons produce in the emulsion are then observed and counted under a microscope. The work is tedious, and the technique is limited by the fact that the ranges of recoil protons with energies less than about 2.5 MeV are too short to produce recognizable tracks.

Film calibration and the use of densitometer readings to obtain dose would appear, in principle, to be straightforward. In practice, however, the procedure is complicated by a number of factors. First, the density produced in film from a given dose of radiation depends on the emulsion type and the particular lot of the manufacturer. Second, firm is affected by environmental conditions, such as exposure to moisture, and by general aging. Elevated temperatures contribute to base fog in an emulsion before development. Third, significant variations in density are introduced by the steps inherent in the film-development process itself. These include the type, concentration, and age of the developing solution as well as the development time and handling through agitation, rinsing, and fixing. Variations from these sources are significantly reduced by applying the following procedure to both the film dosimeters worn by workers and those used for the calibration of the dosimeters. All units should be from the same manufacturer's production lot, stored and handled in similar fashion, developed at the same time under the same conditions, and read with a single densitometer, and even by a single operator. Experience shows that an acceptable degree of reproducibility can be thus attained.

A serious problem of a different nature for dose determination is presented by the strong response of film to low-energy photons. The upper curve in Fig. 10.35 illustrates the relative response (darkening) of film enclosed in thin plastic to a fixed dose of monoenergetic photons as a function of their energy. From about 5 MeV down to 200 keV, the relative response, set at unity in the figure, is flat. Below about 200 keV, the rising photoelectric absorption cross section of the silver in the film leads increasingly to more blackening at the fixed dose than would occur if film were tissue- or air-equivalent. The relative response peaks at around 40 keV and then drops off at still lower energies because of absorption of the photons in the packaging material around the film.

The lower curve in Fig. 10.35 shows the relative response when the incident radiation passes through a cadmium absorber of suitable thickness placed over the film. The absorption of photons in the cadmium filter tends to compensate for the over-response of the film at low energies, while having little effect at high energies, thus extending the usefulness of the badge to lower-energy photons.

Film badges are also used for personnel monitoring of beta radiation, for which there is usually negligible energy dependence of the response. For mixed beta–gamma radiation exposures, the separate contribution of the beta particles is assessed by comparing (1) the optical density behind a suitable filter that absorbs them and (2) the density through a neighboring "open window." The latter consists only of the structural material enclosing the film. Since beta particles have short ranges, a badge that has been exposed to them alone will be darkened behind the open window, but not behind the absorbing filter. Such a finding would also result from exposure to low-energy photons. To distinguish these from beta particles, one

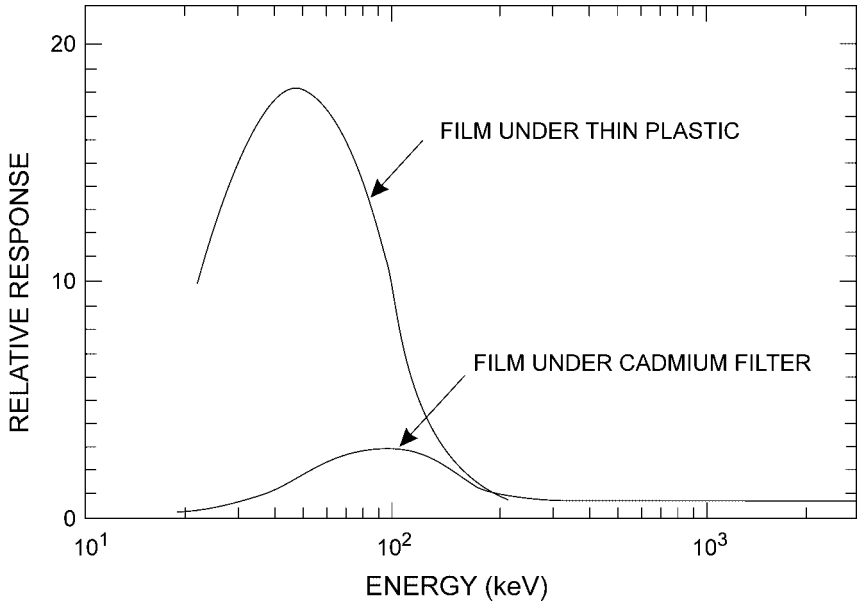

Fig. 10.35 Relative response of film to a fixed dose of monoenergetic photons as a function of energy. Upper curve is for film covered only with thin layer of plastic. Lower curve is for film covered with a cadmium filter to compensate for the over-response to low-energy photons.

can employ two additional filters, one of high and the other of low atomic number, such as silver and aluminum. They should have the same density thickness, so as to be equivalent beta-particle absorbers. The high-Z filter will strongly absorb low-energy photons, which are attenuated less by the low-Z material. The presence of low-energy photons will contribute to a difference in darkening behind the two.

Figure 10.36 shows an exploded view of a multi-purpose film badge used at several sites from about 1960 to 1980. It was designed for routine beta–gamma and neutron personnel monitoring; criticality applications; assessment of a large, accidental gamma dose; and for personal security identification. The laminated picture front, identifying the wearer, was of low-Z material. An assembly, comprised of filters and other units, was placed behind the picture and in front of the film packs, which included both X-ray and nuclear track emulsions. There were four filter areas in the assembly through which radiation could pass to reach the firm. (1) At the window position, the only material traversed in addition to the laminated picture (52 mg cm^{-2}) was the paper wrapper around the film (28 mg cm^{-2}), giving a total density thickness of 80 mg cm^{-2}. (2) The (low-Z) plastic filter had a thickness of about 215 mg cm^{-2}. (3) A gold foil was sandwiched between two pieces of cadmium, each 0.042 cm thick. The combination presented a Cd-Au-Cd absorber thickness of about 1000 mg cm^{-2}. (4) The aluminum filter (275 mg cm^{-2}) was provisionally included at the time for eventual help in determining the effective energy of photon exposures.

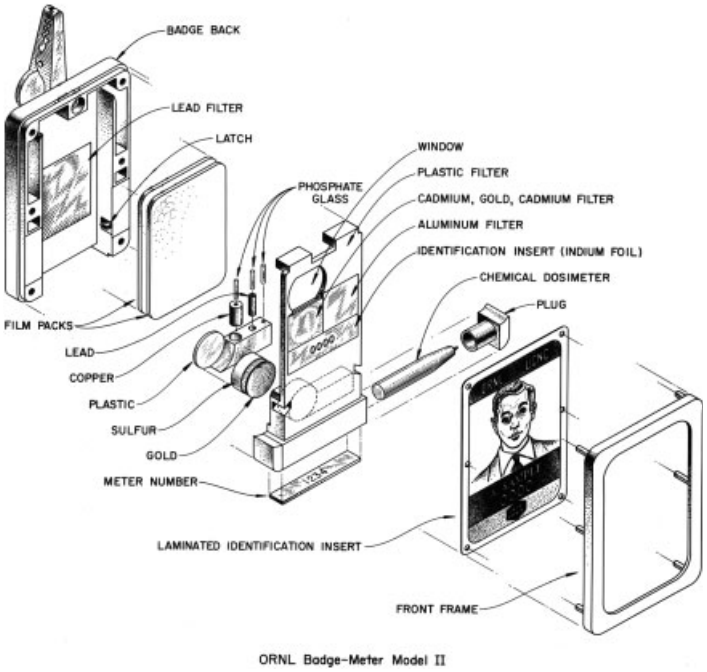

Fig. 10.36 Multi-element film badge in use during the period 1960–1980. [From W. T. Thornton, D. M. Davis, and E. D. Gupton, *The ORNL Badge Dosimeter and its Personnel Monitoring Applications*, Report ORNL-3126, Oak Ridge, TN (1961).]

Readings from badges worn by personnel were analyzed to provide a number of dose quantities, as mandated by regulations, basically in the following ways. The optical density behind the Cd-Au-Cd filter served as a measure of "deep dose" to tissues inside the body. The thickness of the plastic filter plus the picture and film wrapper (300 mg cm^{-2}) corresponded to the 3-mm depth specified for the lens of the eye. Assessment of "skin dose" (specified at a depth of 7 mg cm^{-2}) was based on the Cd-Au-Cd reading and the difference between the densities behind the window and the plastic filter. Depending on the particular beta fields anticipated, an empirical constant was worked out for weighting this difference in the evaluation of the skin dose. The numerical value of the constant was determined from calibration with a particular beta source, often natural uranium. Considerable uncertainty attended determination of skin dose from a badge exposed to an unknown beta–gamma radiation field. The fluence of fast neutrons was proportional to the number of recoil proton tracks observed in the film behind the Cd-Au-Cd filter, which strongly absorbed thermal neutrons. Thermal neutrons produced protons of 0.524 MeV energy in the $^{14}N(n,p)^{14}C$ reaction with nitrogen (Section 9.7) in the emulsions. These were observed in the window portion of the film, and their number was proportional to the fluence of thermal neutrons. These data plus knowledge

of tissue composition and neutron cross sections were applied to estimate neutron doses.

As mentioned, the badge in Fig. 10.36 served other purposes in addition to personal identification and routine radiation monitoring. As an adjunct, three silver meta-phosphate glass rods could measure gamma doses in excess of 100 rad (Section 12.2) and also responded to thermal neutrons. The three rods were surrounded by different shields of lead, copper, and plastic. Comparing their relative responses gave an indication of the effective energy of the photons. The response of the glass rods would be potentially important for accidental exposures to high-level radiation. The chemical dosimeter could enable a swift visual indication of persons exposed in an incident. Several elemental foils with different neutron-activation energy thresholds were included to provide data about the neutron energy spectrum in case of a criticality accident (Section 10.9). A 0.5-g sulfur pellet is activated effectively only by neutrons with energies greater than about 3.2 MeV (Section 9.7). There were two gold foils, which are activated by thermal neutrons. One was enclosed in the Cd-Au-Cd filter and the other was inserted bare behind the sulfur pellet. Significant exposure to neutrons in a criticality accident can be readily identified by the induced activity in the indium foil contained in the badge (Section 9.7). Activity induced in the gold could also serve the same purpose. Although less sensitive than indium, the longer half-life of ^{198}Au (2.696 d) compared with ^{116m}In (54.15 min) is an advantage.

Multi-element film dosimeters for personnel monitoring became largely replaced by thermoluminescent dosimeters (next section) during the 1980s. However, film badges still serve in many applications, such as hospitals, universities, and small laboratories, where radiation fields are relatively uncomplicated and well known.

10.5 Thermoluminescence

In connection with Fig. 10.28, we described how ionizing radiation can produce electron–hole pairs in an inorganic crystal. These lead to the formation of excited states with energies that lie in the forbidden gap when particular added activator impurities are present. In a scintillation detector, it is desirable for the excited states to decay quickly to the ground states, so that prompt fluorescence results. In another class of inorganic crystals, called thermoluminescent dosimeters (TLDs), the crystal material and impurities are chosen so that the electrons and holes remain trapped at the activator sites at room temperature. Placed in a radiation field, a TLD crystal serves as a passive integrating detector, in which the number of trapped electrons and holes depends on its radiation exposure history.

After exposure, the TLD material is heated. As the temperature rises, trapped electrons and holes migrate and combine, with the accompanying emission of photons with energies of a few eV. Some of the photons enter a photomultiplier tube and produce an electronic signal. The sample is commonly processed in a TLD

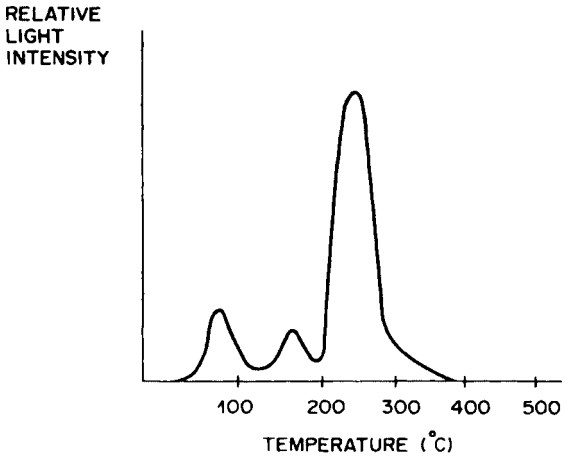

Fig. 10.37 Typical TLD glow curve.

reader, which automatically heats the material, measures the light yield as a function of temperature, and records the information in the form of a glow curve, such as that shown in Fig. 10.37. Typically, several peaks occur as traps at different energy levels are emptied. The total light output or the area under the glow curve can be compared with that from calibrated TLDs to infer radiation dose. All traps can be emptied by heating to sufficiently high temperature, and the crystal reused.

A number of TLD materials are in use. Manganese-activated calcium sulfate, $CaSO_4 : Mn$, is sensitive enough to measure doses of a few tens of μrad. Its traps are relatively shallow, however, and it has the disadvantage of "fading" significantly in 24 h. $CaSO_4 : Dy$ is better. Another popular TLD crystal is LiF, which has inherent defects and impurities and needs no added activator. It exhibits negligible fading and is close to tissue in atomic composition. It can be used to measure gamma-ray doses in the range of about 0.01–1000 rad. Other TLD materials include $CaF_2 : Mn$, $CaF_2 : Dy$, and $Li_2B_4O_7 : Mn$.

Figure 10.38 shows schematic drawings of two TLD personnel dosimeters. The beta–gamma system on the left has four LiF chips. Elements 1, 2, and 3 are Harshaw TLD-700 material, which is essentially pure ^{7}LiF and, therefore, insensitive to neutrons.[2)] The first chip has a thickness of 0.015 in = 0.38 mm, and is situated behind 1,000 mg cm^{-2} of Teflon and plastic to measure the regulatory "deep dose" (Section 14.9). Chip 2 is set behind a thin absorber and a 0.004 in = 0.10 mm layer of copper, giving a total thickness of 333 mg cm^{-2}. The copper filters out low-energy photons while transmitting some beta particles. Its response, compared with that of chip 3 behind a thin absorber ("open window") for low-energy photon discrimination, is used for the assessment of shallow dose (Section 14.9). The remaining element 4 consists of TLD-600, which is enriched to about 96% in the isotope ^{6}Li. This chip is sensitive to thermal neutrons and is at the regulatory depth of the lens of the eye (300 mg cm^{-2}). If a person wearing the dosimeter is exposed to fast neu-

2 Natural lithium is 92.5% ^{7}Li and 7.5% ^{6}Li.

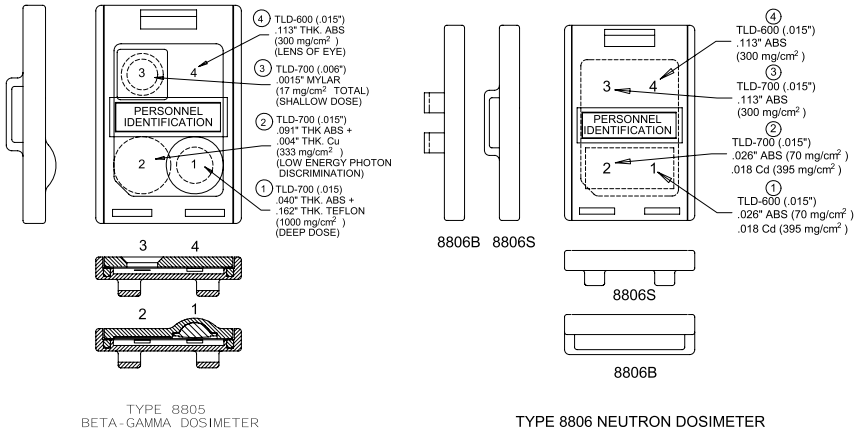

Fig. 10.38 Schematic views of beta–gamma (left) and neutron (right) TLD dosimeters. (Courtesy Thermo Electron Corp.)

trons, some will be moderated by the body and detected as slow neutrons only in chip 4 of the dosimeter, thus furnishing evidence of neutron exposure.

When a potential for exposure to neutrons exists, a special TLD dosimeter, such as that shown on the right in Fig. 10.38, should be employed. Readings from the pairs of TLD-600 and TLD-700 elements, one sensitive and the other insensitive to neutrons, can be compared. Since their responses to gamma rays are identical, differences can be attributed to neutrons. The cadmium filters for chips 1 and 2 absorb incident thermal neutrons. Differences in their readings, therefore, are associated with fast neutrons. Without the cadmium filters, differences between elements 3 and 4 indicate total (fast-plus-thermal) neutron exposure.

The beta–gamma dosimeter of Fig. 10.38 and its system of filters is displayed in Fig. 10.39. Thermoluminesent dosimeters can be processed by automated readout systems, which can transfer results to a central computer system for dosimetry records. Computer algorithms have been written to unfold the required dose assessments for individuals from the readings obtained from the different chips. Laboratory accreditation is provided through the National Voluntary Laboratory Accreditation Program (NVLAP).

10.6 Other Methods

Particle Track Registration

A number of techniques have been devised for directly observing the tracks of individual charged particles. Neutron dosimetry with the film badge described in Section 10.4 utilized neutron-sensitive emulsions in which the tracks of recoil pro-

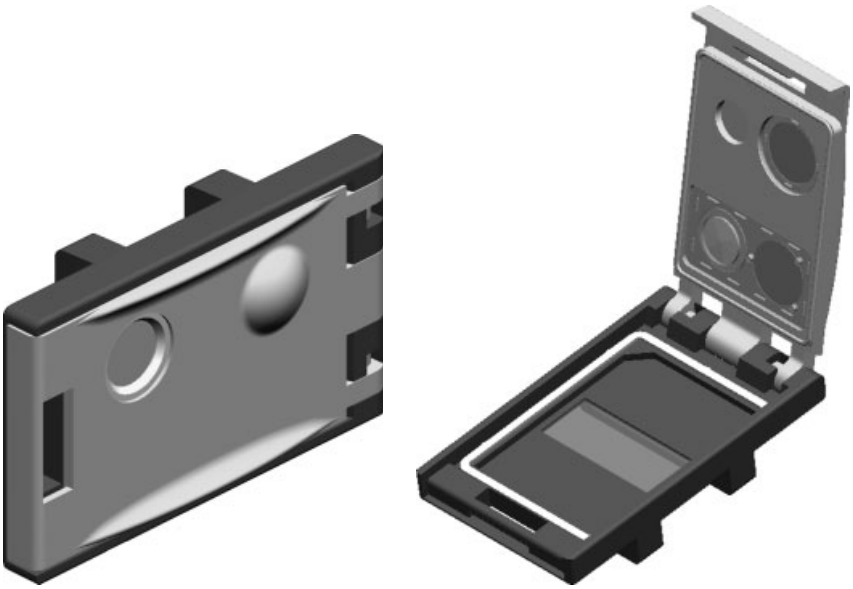

Fig. 10.39 Left: closed TLD dosimeter. Right: open dosimeter, showing four filter areas, chips removed. (Courtesy Thermo Electron Corp.)

tons from the elastic scattering of fast neutrons could be counted and analyzed. Figure 5.1 shows an example of alpha- and beta-particle tracks in photographic film. In the cloud chamber, moisture from a supersaturated vapor condenses on the ions left in the wake of a passing charged particle, rendering the track visible. In the bubble chamber, tiny bubbles are formed as a superheated liquid starts to boil along a charged particle's track. Another device, the spark chamber, utilizes a potential difference between a stack of plates to cause a discharge along the ionized path of a charged particle that passes through the stack.

Track etching is possible in some organic polymers and in several types of glasses. A charged particle causes radiation damage along its path in the material. When treated chemically or electrochemically, the damaged sites are attacked preferentially and made visible, either with a microscope or the unaided eye. Track etching is feasible only for particles of high LET. The technique is widely used in neutron dosimetry (e.g., CR-39 detectors). Although neutral particles do not produce a trail of ions, the tracks of the charged recoil particles they produce can be registered by techniques discussed here.

Optically Stimulated Luminescence

Optically stimulated luminescence (OSL) shares some similarities and some contrasts with thermoluminescence. A number of materials exhibit both phenomena. Under irradiation, electrons become trapped in long-lived excited states of doped crystals. With TLDs, dose is inferred from the amount of light emitted under thermal stim-

ulation. With OSL, the light emission is caused by optical stimulation. Reading a TLD empties all of the trapped-electron states, erasing the primary record and returning the dosimeter to its original condition for reuse. Reading with OSL, on the other hand, depletes relatively little of the stored charge, essentially preserving the primary record and enabling the dosimeter to be read again. The variable stimulation power with OSL can be used to advantage to achieve sensitivity over a wide range of doses.

Although a decades-old idea, practical use of OSL for dosimetry became a reality with the development of the Luxel® personnel dosimeters by Landau, Inc. in the late 1990s. The detector material is aluminum oxide, grown in the presence of carbon, Al_2O_3 : C. (Crystals with different dopants can be fabricated for specialized applications.) Figure 10.40 displays a Luxel® dosimeter. A thin Al_2O_3 strip is sandwiched between a multi-element, sealed filter pack. As with film and TLD, the different filters are used to provide specific information about mixed radiation fields for personnel dose assessment. The individual read outs are fed into a computer algorithm that estimates the regulatory deep and shallow doses. Neutron dose assessment can be added by the inclusion of an optional CR-39 detector in the dosimeter, which is analyzed by track etching and counting.

Landauer employs two dosimeter read-out methods. Since the induced light emitted from the detector must be measured in the presence of the stimulating light, it is essential that the two light sources not be mixed. In one method, the stimulation is caused by a pulsed laser and the emission signal is read between pulses. The other method employs continuous stimulation by light-emitting diodes (LEDs) or CW (continuous-wave) laser, and the measurement of the light emitted from the detector at wavelengths outside the LED or laser spectrum. The pulsed system is more expensive and more complex, but considerably faster than the continuous-stimulation method.

Direct Ion Storage (DIS)

Direct Ion Storage (DIS) has been recently developed into an important basis for a personal dosimeter. A predetermined amount of electric charge is placed on the floating plate of a nonvolatile solid-state DIS memory cell. The charge is tunneled onto the gate through oxide-silicon material that surrounds it. At normal temperatures, the stored charge is trapped permanently on the gate because of the extremely low probability of thermal excitations of electrons through the adjacent material. The amount of charge stored on the gate can be "read" without disturbing it by making conductivity measurements with the cell. In this configuration the device is not sensitive to ionizing radiation, because the low mobility of charge carriers in the oxide prevents neutralization of charge on the gate before recombination.

To make a dosimeter, the memory cell is enclosed within a conductive wall, forming in a small ($\sim$10 cm^3) ionization chamber, containing air or other gas. The oxide layer is provided with a small opening to make contact between the floating plate and the chamber gas. Radiation now produces ion pairs with high mobility in the

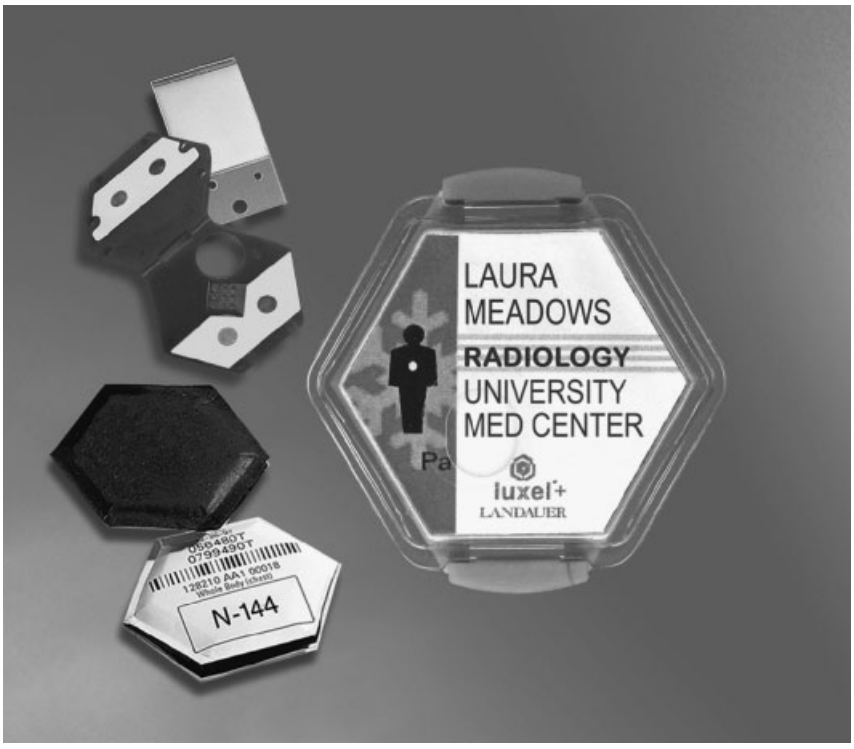

(a)

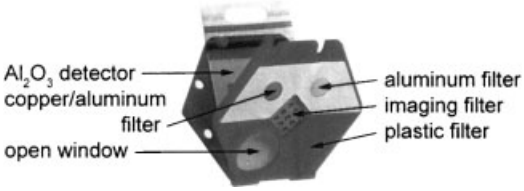

(b)

Fig. 10.40 Luxel® personnel dosimeter. (b) Filter pack, showing detector, filters, and open window. (Courtesy Landauer, Inc.)

gas. Electric fields direct the charge carriers through the hole in the oxide layer to reduce the charge initially stored on the floating plate. DIS dosimeters are calibrated to provide dose assessment from the measured loss of charge. Depending on the radiation fields to be monitored, characteristics of the wall material and thickness as well as other factors can be varied to fit the application.

The basic design of the direct ion storage dosimeter gives it the flat energy response of an ionization chamber. It has instant, non-destructive read-out. The dosimeter shown in Fig. 10.41 with its reader is rugged, light (20 g without holder),

(a) (b)

Fig. 10.41 (a) Direct ion storage personal dosimeter and (b) reader. (Courtesy RADOS Technology.)

and waterproof. It measures photon dose equivalent in the range 1–40 μSv and beta dose equivalent from 10 μSv–40 Sv.

Radiophotoluminescence

The film badge in Fig. 10.36 contained three silver meta-phosphate glass rods to measure large photon doses ($\geq$100 rad = 1 Gy), as might occur in an accident. Energy absorbed from the ionizing radiation leads to the migration of electrons to permanent sites associated with the silver in the glass. As a result, new absorption frequencies are produced, and the glass will fluoresce under exposure to ultraviolet light. The fluorescence yield can then be compared with calibrated standards to infer dose. Since the fluorescence does not change the glass, the read-out is nondestructive. Although radiophotoluminescence has been used for routine personnel dosimetry, it has generally been limited to high-dose applications.

Chemical Dosimeters

Radiation produces chemical changes. One of the most widely studied chemical detection systems is the Fricke dosimeter, in which ferrous ions in a sulfate solution are oxidized by the action of radiation. As in all aqueous chemical dosimeters, radiation interacts with water to produce free radicals (e.g., H and OH), which are highly reactive. The OH radical, for example, can oxidize the ferrous ion directly: $Fe^{2+} + OH \rightarrow Fe^{3+} + OH^{-}$. After irradiation, aqueous chemical dosimeters can be analyzed by titration or light absorption. The useful range of the Fricke dosimeter is from about 40 to 400 Gray (Gy). The dose measurements are accurate and absolute. The aqueous system approximates soft tissue.

Other chemical-dosimetry systems are based on ceric sulfate, oxalic acid, or a combination of ferrous sulfate and cupric sulfate. Doses of the order of 0.1 Gy can be measured chemically with some chlorinated hydrocarbons, such as chloroform. Higher doses result in visible color changes in some systems.

Calorimetry

The energy imparted to matter from radiation is usually efficiently converted into heat. (Radiation energy can also be expended in nuclear transformations and chemical changes.) If the absorber is thermally insulated, as in a calorimeter, then the temperature rise can be used to infer absorbed dose absolutely. However, a relatively large amount of radiation is required for calorimetric measurements. An absorbed energy of 4180 $\mathrm{J\,kg^{-1}}$ (= 4180 Gy) in water raises the temperature only 1°C (Problem 39). Because they are relatively insensitive, calorimetric methods in dosimetry have been employed primarily for high-intensity radiation beams, such as those used for radiotherapy. Calorimetric methods are also utilized for the absolute calibration of source strength.

Cerenkov Detectors

When a charged particle travels in a medium faster than light, it emits visible electromagnetic radiation, analogous to the shock wave produced in air at supersonic velocities. The speed of light in a medium with index of refraction n is given by c/n, where c is the speed of light in a vacuum. Letting $v = \beta c$ represent the speed of the particle, we can express the condition for the emission of Cerenkov radiation as $\beta c > c/n$, or

$$\beta n > 1. \tag{10.8}$$

The light is emitted preferentially in the direction the particle is traveling and is confined to a cone with vertex angle given by $\cos\theta = 1/\beta n$. It follows from (10.8) that the threshold kinetic energy for emission of Cerenkov light by a particle of rest mass M is given by (Problem 40)

$$T = Mc^2\left(\frac{n}{\sqrt{n^2-1}} - 1\right). \tag{10.9}$$

The familiar "blue glow" seen coming from a reactor core [e.g., Figs. 9.1 and 9.2(b)] is Cerenkov radiation, emitted by energetic beta particles traveling faster than light in the water.

Cerenkov detectors are employed to observe high-energy particles. The emitted radiation can also be used to measure high-energy beta-particle activity in aqueous samples.

10.7
Neutron Detection

Slow Neutrons

Neutrons are detected through the charged particles they produce in nuclear reactions, both inelastic and elastic. In some applications, pulses from the charged particles are registered simply to infer the presence of neutrons. In other situations, the neutron energy spectrum is sought, and the pulses must be further analyzed. For slow neutrons (kinetic energies $T \lesssim 0.5$ eV), detection is usually the only requirement. For intermediate (0.5 eV $\lesssim T \lesssim$ 0.1 MeV) and fast ($T \gtrsim 0.1$ MeV) neutrons, spectral measurements are frequently needed. We discuss slow-neutron detection methods first.

Table 10.2 lists the three most important nuclear reactions for slow-neutron detection. The reaction-product kinetic energies and cross sections are given for capture of thermal neutrons (energy = 0.025 eV). Since the incident kinetic energy of a thermal neutron is negligible, the sum of the kinetic energies of the reaction products is equal to the Q value itself. Given Q, equations analogous to Eqs. (3.18) and (3.19) can be applied to calculate the discrete energies of the two products, leading to the values given in Table 10.2. We shall describe slow-neutron detection by means of these reactions and then briefly discuss detection by fission reactions and foil activation.

^{10}B(n,α)

One of the most widely used slow-neutron detectors is a proportional counter using boron trifluoride (BF_3) gas. For increased sensitivity, the boron is usually highly enriched in ^{10}B above its 19.7% natural isotopic abundance. If the dimensions of the tube are large compared with the ranges of the reaction products, then pulse heights at the Q values of 2.31 MeV and 2.79 MeV should be observed with areas

Table 10.2 Reactions Used for Slow-Neutron Detection (Numerical Data Apply to Thermal-Neutron Capture)

Reaction	Q Value (MeV)	Product Kinetic Energies (MeV)	Cross Section (Barns)
$^{10}_{5}\mathrm{B} + {}^{1}_{0}\mathrm{n} \rightarrow {}^{7}_{3}\mathrm{Li}^{*} + {}^{4}_{2}\mathrm{He}$ (96%)	2.31	$T_{\mathrm{Li}} = 0.84$ $T_{\mathrm{He}} = 1.47$	3840
$^{10}_{5}\mathrm{B} + {}^{1}_{0}\mathrm{n} \rightarrow {}^{7}_{3}\mathrm{Li} + {}^{4}_{2}\mathrm{He}$ (4%)	2.79	$T_{\mathrm{Li}} = 1.01$ $T_{\mathrm{He}} = 1.78$	
$^{6}_{3}\mathrm{Li} + {}^{1}_{0}\mathrm{n} \rightarrow {}^{3}_{1}\mathrm{H} + {}^{4}_{2}\mathrm{He}$	4.78	$T_{\mathrm{H}} = 2.73$ $T_{\mathrm{He}} = 2.05$	940
$^{3}_{2}\mathrm{He} + {}^{1}_{0}\mathrm{n} \rightarrow {}^{3}_{1}\mathrm{H} + {}^{1}_{1}\mathrm{H}$	0.765	$T_{3\mathrm{H}} = 0.191$ $T_{1\mathrm{H}} = 0.574$	5330

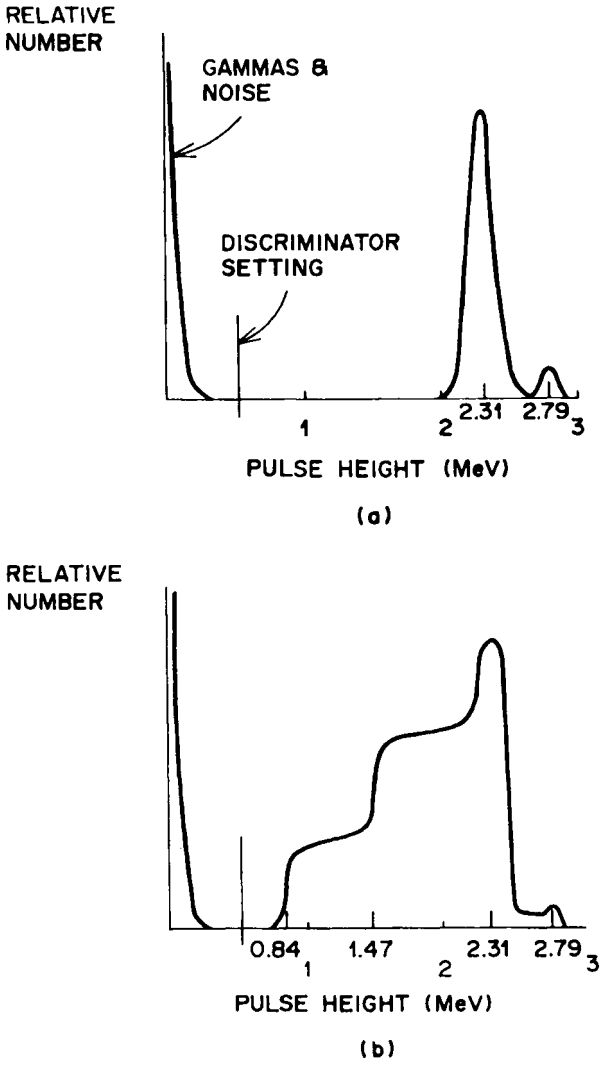

Fig. 10.42 (a) Idealized thermal-neutron pulse-height spectrum from large BF_3 tube in which reaction products are completely absorbed in the gas. (b) Spectrum from tube showing wall effects.

in the ratio 96 : 4, as shown in Fig. 10.42(a). With most practical sizes, however, a significant number of Li nuclei and alpha particles enter the wall of the tube, and energy lost there is not registered. Since the two reaction products separate "back-to-back" to conserve momentum, when one strikes the wall the other is directed away from it. This wall effect introduces continua to the left of the peaks. As sketched in Fig. 10.42(b), one continuum takes off from the peak at 2.31 MeV and is approximately flat down to 1.47 MeV. (A similar continuum occurs below

the small peak at 2.79 MeV.) Over this interval, the total energy (1.47 MeV) of the alpha particle is absorbed in the gas while only part of the energy of the Li nucleus is absorbed there, the rest going into the wall. Below 1.47 MeV, the spectrum again drops and is approximately flat down to the energy 0.84 MeV of the Li recoil. Pulses occur here when the Li nucleus stops in the gas and the alpha particle enters the wall.

The BF_3 proportional counter can discriminate against gamma rays, which are usually present with neutrons and produce secondary electrons that ionize the gas. Compared with the neutron reaction products, electrons produced by the photons are sparsely ionizing and give much smaller pulses. As indicated in Fig. 10.42(a), amplitude discrimination can be used to eliminate these counts as well as electronic noise if the gamma fluence rate is not too large. In intense gamma fields, however, the pileup of multiple pulses from photons can become a problem.

In other counter designs, a boron compound is used to line the interior walls of the tube, in which another gas, more suitable for proportional counting than BF_3, is used. Boron-loaded scintillators (e.g., ZnS) are also employed for slow-neutron detection.

^{6}Li(n,α)

As shown in Table 10.2, this reaction, compared with ^{10}B(n,α), has a higher Q value (potentially better gamma-ray discrimination), but lower cross section (less sensitivity). The isotope ^{6}Li is 7.42% abundant in nature, but lithium enriched in ^{6}Li is available.

Lithium scintillators are frequently used for slow-neutron detection. Analogous to NaI(Tl), crystals of LiI(Eu) can be employed. They can be made large compared with the ranges of the reaction products, so that the pulse-height spectra are free of wall effects. However, the scintillation efficiency is then comparable for electrons and heavy charged particles, and so gamma-ray discrimination is much poorer than with BF_3 gas.

Lithium compounds can be mixed with ZnS to make small detectors. Because secondary electrons produced by gamma rays easily escape, gamma-ray discrimination with such devices is good.

^{3}He(n,p)

This reaction has the highest cross section of the three in Table 10.2. Like the BF_3 tube, the ^{3}He proportional counter exhibits wall effects. However, ^{3}He is a better counter gas and can be operated at higher pressures with better detection efficiency. Because of the low value of Q, though, gamma discrimination is worse.

(n,f)

Slow-neutron-induced fission of ^{233}U, ^{235}U, or ^{239}Pu is utilized in fission counters. The Q value of ~200 MeV for each is large. About 165 MeV of this energy is converted directly into kinetic energy of the heavy fission fragments. Fission pulses are extremely large, enabling slow-neutron counting to be done at low levels, even in a high background. Most commonly, the fissile material is coated on the in-

ner surface of an ionization chamber. A disadvantage of fissionable materials is that they are alpha emitters, and one must sometimes contend with the pileup of alpha-particle pulses.

Activation Foils

Slow neutrons captured by nuclei induce radioactivity in a number of elements, which can be made into foils for neutron detection. The amount of induced activity will depend on a number of factors—the element chosen, the mass of the foil, the neutron energy spectrum, the capture cross section, and the time of irradiation. Examples of thermal-neutron activation-foil materials include Mn, Co, Cu, Ag, In, Dy, and Au.

Intermediate and Fast Neutrons

Nuclear reactions are also important for measurements with intermediate and fast neutrons. In addition, neutrons at these speeds can, by elastic scattering, transfer detectable kinetic energies to nuclei, especially hydrogen. Elastic recoil energies are negligible for slow neutrons. Detector systems can be conveniently discussed in four groups—those based on neutron moderation, nuclear reactions, elastic scattering alone, and foil activation. Recent developments also include bubble detectors.

Neutron Moderation

Two principal systems in this category have been developed: the long counter and moderating spheres enclosing a small thermal-neutron detector. A cross section of the cylindrical long counter is shown in Fig. 10.43. This detector, which is one of the oldest still in use, can be constructed to give nearly the same response from a neutron of any energy from about 10 keV to 5 MeV. The long counter contains a BF_3 tube surrounded by an inner paraffin moderator, as shown. The instrument is sensitive to neutrons incident from the right. Those from other directions are either reflected or thermalized by the outer paraffin jacket and then absorbed in the B_2O_3 layer. Neutrons that enter from the right are slowed down in the inner paraffin moderator, high-energy neutrons reaching greater depths on the average than low-energy ones. With this arrangement, the probability that a moderated neutron will enter the BF_3 tube and be registered does not depend strongly on the initial energy with which it entered the counter. Holes on the front face make it easier for neutrons with energies <1 MeV to penetrate past the surface, from which they might otherwise be reflected. The long counter does not measure neutron spectra.

Neutron spectral information can be inferred by the use of polyethylene moderating spheres (Bonner spheres) of different diameters with small lithium iodide scintillators at their centers. A series of five or more spheres, ranging in diameter from 2 to 12 in., is typically used. The different sizes provide varying degrees of moderation for neutrons of different energies. The response of each sphere is calibrated for monoenergetic neutrons from thermal energy to 10 MeV or more.

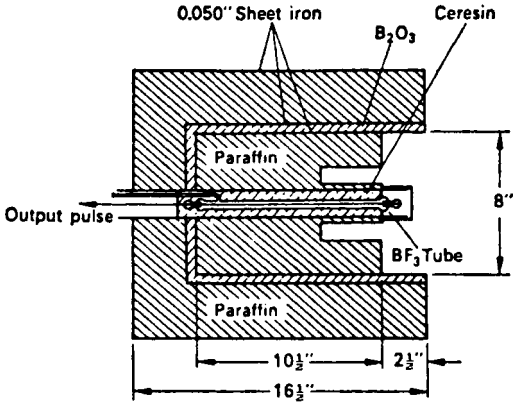

Fig. 10.43 The original long counter of Hanson and McKibben. [Reprinted with permission from A. O. Hanson and M. L. McKibben, "A Neutron Detector Having Uniform Sensitivity from 10 keV to 5 MeV," *Phys. Rev.* **72**, 673 (1947). Copyright 1947 by the American Physical Society.]

The spheres are then exposed in an unknown neutron field and the count rates measured. An unfolding procedure is used to infer information about the neutron spectrum from knowledge of the calibration curves and the measured count rates. Because the unfolding procedure does not yield very precise results, this method is not widely used for spectral measurements. With a relatively large sphere, it is found that the response as a function of neutron energy is similar to the dose equivalent per neutron. It therefore serves as a neutron rem meter in many applied health physics operations. Such an instrument is shown in Fig. 10.44.

Nuclear Reactions

The ^{6}Li(n,α) and ^{3}He(n,p) reactions are the only ones of major importance for neutron spectrometry. Ideally, an incident neutron of energy T that undergoes a reaction causes a detector to register a peak at an energy $Q + T$. In practice, many times another peak also occurs at an energy Q due to neutrons that have been slowed by multiple scattering in building walls and shielding around the detector. Slow-neutron cross sections can be orders of magnitude larger than at higher energies. The additional peak at Q is sometimes called the epithermal peak.

Crystals of LiI(Eu) are used in neutron spectroscopy. However, the nonlinearity of their response with the energy of the reaction products (tritons and alpha particles) is a serious handicap. Lithium-glass scintillators are also in use, principally as fast responding detectors in neutron time-of-flight measurements. In another type of neutron spectrometer, a thin LiF sheet is placed between two semiconductor diodes. At relatively low neutron energies T, the recoil products will tend to be ejected back-to-back, giving coincidence counts in both semiconductors with a total pulse height of $Q + T$, from which T can be ascertained.

In the ^{3}He(n,p) proportional counter, monoenergetic neutrons of energy T produce a peak at energy $T + 0.765$ MeV, as illustrated in Fig. 10.45. The epithermal

Fig. 10.44 Instrument for measuring neutron dose-equivalent rate. A ^{3}He proportional counter tube is located at the center of a polyethylene moderator sphere. The cylindrical tube has approximately equal height and diameter to minimize directional dependence of the response. Sensitivity is about 3 counts per nSv (3 counts per μrem) in the energy range 1 to 10 MeV. Good gamma discrimination. (Courtesy Berthold Technologies USA, LLC.)

peak is also shown at the energy $Q = 0.765$ MeV. In addition to these peaks from the reaction products, one finds a continuum of pulse heights from recoil ^{3}He nuclei that elastically scatter incident neutrons. It follows from Eq. (9.3) that the maximum kinetic energy that a neutron of mass $m = 1$ and kinetic energy T can transfer to a helium nucleus of mass $M = 3$ is

$$T_{\max} = \frac{4mM}{(m+M)^2}T = \frac{4 \times 1 \times 3}{(1+3)^2}T = \frac{3}{4}T. \tag{10.10}$$

The elastic continuum in Fig. 10.45 thus extends up to the energy $0.75T$. Wall effects can be reduced in the ^{3}He proportional counter by using gas pressures of several atmospheres and also by adding a heavier gas (e.g., Kr).

Elastic Scattering

A number of instruments are based on elastic scattering alone, especially from hydrogen. As discussed in Section 9.5, a neutron can lose all of its kinetic energy T in a single head-on collision with a proton. Also, since n–p scattering is isotropic

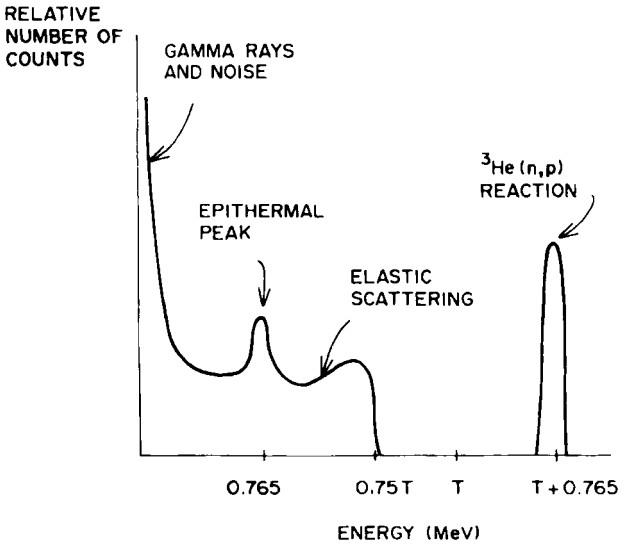

Fig. 10.45 Pulse-height spectrum from ^{3}He proportional counter for monoenergetic neutrons of energy T.

in the center-of-mass system for neutron laboratory energies up to ~10 MeV, the average energy imparted to protons by neutrons in this energy range is $T/2$ (Section 9.6).

Organic proton-recoil scintillators are available for neutron spectrometry in a variety of crystal, plastic, and liquid materials. The full proton recoil energies can be caught in these scintillators. Complications in the use of proton-recoil scintillators include nonlinearity of response, multiple neutron scattering, and competing nuclear reactions. For applications in mixed fields, the gamma response can, in principle, be separated electronically from the neutron response on the basis of quicker scintillation.

Proportional counters have been designed with hydrocarbon gases, such as CH_4. These have inherently lower detection efficiencies than solid-state devices, but offer the potential for better gamma discrimination. Wall effects can be important. Proportional counters have also been constructed with polyethylene or other hydrogenous material surrounding the tube. One such device, based on the Bragg–Gray principle, will be discussed in Section 12.6.

A proton-recoil telescope, illustrated in Fig. 10.46, can be used to accurately measure the spectrum of neutrons in a collimated beam. At an angle θ, the energy T_p of a recoil proton from a thin target struck by a neutron of incident energy T is, by Eq. (9.5),

$$T_p = T\cos^2\theta. \tag{10.11}$$

The $E(-dE/dx)$ coincidence particle identifier (Fig. 10.27) can be used to reduce background, eliminate competing events, and measure T_p.

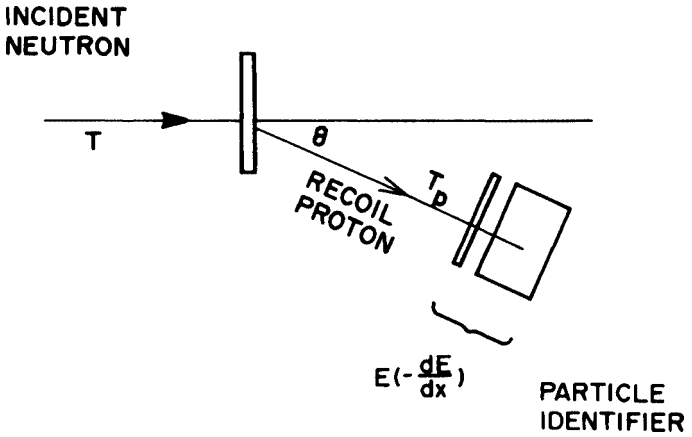

Fig. 10.46 Arrangement of proton-recoil telescope for measuring spectrum of a neutron beam.

Neutron spectra can also be inferred from the observed range distribution of recoil protons in nuclear track emulsions. Neutrons with at least several hundred keV of energy are needed to produce protons with recognizable tracks.

Threshold Foil Activation

Like low-energy neutrons, intermediate and fast neutrons can be detected by the radioactivity they induce in various elements. With many nuclides, a threshold energy exists for the required nuclear reaction. When foils of several nuclides are simultaneously exposed to a neutron field, differences in the induced activity between them can be used to obtain information about the neutron energy spectrum as well as the fluence.

As described at the end of Section 9.8, the activity induced in a foil or other target is a combined result of (1) the neutron fluence (and fluence rate) at energies above threshold and (2) the energy-dependent cross section for the reaction. Activation provides an estimate of neutron fluence at an effective threshold energy above the minimum given by Eq. (9.29). The effective threshold energy is thus only an approximate concept; for a given material, different specific values can be found in the literature. Table 10.3 lists some reactions and their effective threshold energies used for fast-neutron detection. As an example, if an exposed aluminum foil shows induced activity from ^{27}Mg and a simultaneously exposed cobalt foil shows no induced activity from ^{56}Mn, then one can infer that neutrons with energies 3.8 MeV < T < 5.2 MeV were present. To obtain accurate spectral data from threshold-detector systems, one must take into account such factors as the masses of the particular isotopes in the foils, their neutron cross sections as functions of energy, the exposure history of the foils, and the half-lives of the induced radioisotopes.

Bubble Detectors

The popular bubble detector is a unique and important personal neutron dosimeter. Figure 10.47 shows a pair of detectors, one exposed to neutrons and the other unexposed. The basic dosimeter consists of 8 cm^3 of a clear polymer in which tens

Table 10.3 Reactions for Threshold Activation Detectors of Neutrons

Reaction	Effective Threshold (MeV)
$^{115}In(n,n')^{115m}In$	0.5
$^{58}Ni(n,p)^{58}Co$	1.9
$^{27}Al(n,p)^{27}Mg$	3.8
$^{56}Fe(n,p)^{56}Mn$	4.9
$^{59}Co(n,\alpha)^{56}Mn$	5.2
$^{24}Mg(n,p)^{24}Na$	6.0
$^{197}Au(n,2n)^{196}Au$	8.6

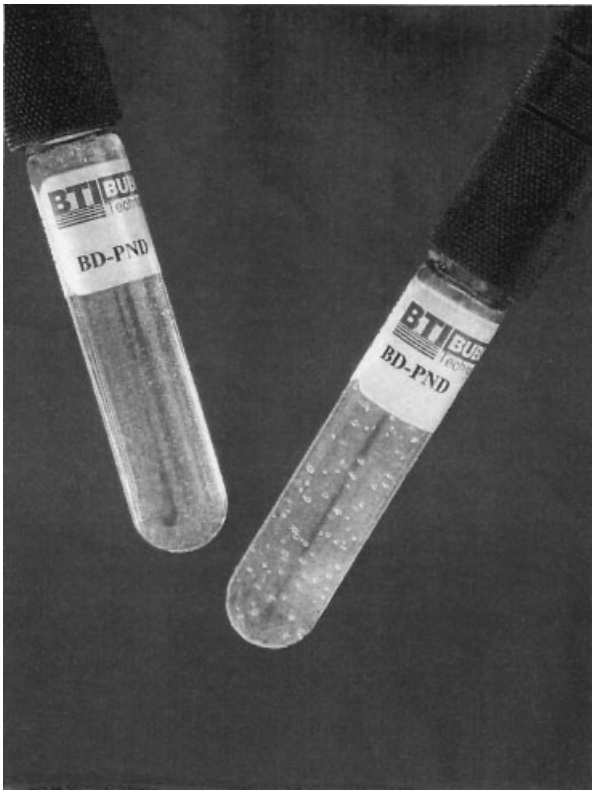

Fig. 10.47 Bubble detectors before and after exposure to neutrons. (Courtesy H. Ing, Bubble Technology Industries, Inc.)

of thousands of microscopic droplets of a superheated liquid (Freon-12, for example) are dispersed. A liquid that continues to exist as such at temperatures above its normal boiling point is said to be superheated. Under this condition, a sudden disturbance in the droplet, such as the passage of a charged particle generated from a neutron interaction, can produce a boiling, explosive phase transition into a vapor. Droplets are instantly transformed into small, visible bubbles in the dosimeter.

They are fixed indefinitely in the polymer, and can be counted visually or with an automatic reader. Dosimeter properties can be adjusted to meet different objectives by varying the polymer and the detecting liquid. After reading, the bubbles can be made to disappear by recompression through a screw-cap assembly on the unit, thus restoring it to the unexposed state.

The bubble detector is a sensitive, passive neutron dosimeter. Although commonly manufactured to have about one bubble per mrem of fast-neutron dose equivalent (Section 12.2), it has been produced with up to three orders of magnitude higher sensitivity. Its threshold neutron energy of about 100 keV is lower than that of nuclear-track film. The tissue-equivalent dose response is flat from approximately 200 keV to more than 15 MeV. It is isotropic and completely insensitive to gamma radiation. A compound containing ^{6}Li and dispersed in the polymer can be used to monitor thermal neutrons. Sets of bubble detectors, fabricated with different neutron-energy thresholds, have been employed to obtain spectral information for dosimetry.

10.8 Suggested Reading

The best sources of information in the diverse and rapidly expanding field of radiation detection and instrumentation are on the World Wide Web. Detailed data can be found on virtually any current or historic topic. The following publications are suggested as supplements to this chapter.

1 Frame, Paul W., "A History of Radiation Detection Instrumentation," *Health Phys.* **88**, 613–637 (2005). [This important publication appears in the issue commemorating the 50th anniversary of the Health Physics Society. It provides a comprehensive, in-depth review of the history of radiation detection from early days through modern technology. Extensive bibliography. The numerous photographs in the article are of instruments in Oak Ridge Associated Universities' Historical Instrumentation Collection, which is managed by Dr. Frame. The collection can be accessed on-line at http://www.orau.org/ptp/museumdirectory.htm.]

2 ICRU Report 31, *Average Energy Required to Produce an Ion Pair*, International Commission on Radiation Units and Measurements, Washington, DC (1979).

3 Knoll, Glenn F., *Radiation Detection and Measurement*, 3rd Ed., Wiley, New York (2000). [This authoritative textbook covers many of the subjects of this chapter in detail.]

4 Poston, John W., Sr., "External Dosimetry and Personnel Monitoring," *Health Phys.* **88**, 557–564 (2005). [This review is another in the issue commemorating the 50th anniversary of the Health Physics Society. Radiation detection is discussed with emphasis on personnel dosimetry. Accompanying historical information is included. Bibliography.]

10.9 Problems

1. How many electrons are collected per second in an ionization chamber when the current is 5×10^{-14} A? What is the rate of energy absorption if $W = 29.9$ eV ip^{-1}?

2. How many ion pairs does a 5.6-MeV alpha particle produce in N_2 (Fig. 10.2)?
3. Why do the W values for heavy charged particles increase at low energies (Fig. 10.2)?
4. A beam of alpha particles produced a current of 10^{-14} A in a parallel-plate ionization chamber for 8 s. The chamber contained air at STP.
   (a) How many ion pairs were produced?
   (b) How much energy did the beam deposit in the chamber?
   (c) If the chamber volume was 240 cm^3, what was the energy absorbed per unit mass in the chamber gas (1 gray absorbed dose = 1 J kg^{-1})?
5. A 10-cm^2 beam of charged particles is totally absorbed in an ionization chamber, producing a saturation current of 10^{-6} A. If $W = 30$ eV ip^{-1}, what is the average beam intensity in units of eV cm^{-2} s^{-1}?
6. A 5-MeV alpha-particle beam of cross-sectional area 2 cm^2 is stopped completely in an ionization chamber, producing a current of 10 μA under voltage saturation conditions.
   (a) If $W = 32$ eV ip^{-1}, what is the intensity of the beam?
   (b) What is the fluence rate?
7. A thin radioactive source placed in an ionization chamber emits 10^6 alpha particles per second with energy 3.81 MeV. The particles are completely stopped in the gas, for which $W = 36$ eV ip^{-1}. Calculate
   (a) the average number of ion pairs produced per second
   (b) the current that flows under saturation conditions
   (c) the amount of charge collected in 1 h.
8. Assume that the W values for protons and carbon-recoil nuclei are both 30 eV ip^{-1} in C_2H_4 gas. What is the maximum number of ion pairs that can be produced by a 3-MeV neutron interacting elastically with (a) H or (b) C?
9. An alpha-particle source is fabricated into a thin foil. Placed first in a 2π gas-flow proportional counter, it shows only a single pulse height and registers 7080 counts min^{-1} (background negligible). The source is next placed in 4π geometry in an air ionization chamber operated under saturation conditions, where it produces a current of 5.56×10^{-12} A. Assume that the foil stops the recoil nuclei following alpha decay but absorbs a negligible amount of energy from the alpha particles.
   (a) What is the activity of the source?
   (b) What is the alpha-particle energy?
   (c) Assume that the atomic mass number of the daughter nucleus is 206 and calculate its recoil energy.

10. A ^{210}Po source is placed in an air ionization chamber, and a saturation current of 8×10^{-12} A is observed. Assume that the ionization is due entirely to 5.30-MeV alpha particles stopping in the chamber. How many stop per second?

11. An ionization chamber is simultaneously bombarded by a beam of 8×10^6 helium ions per second and a beam of 1×10^8 carbon ions per second. The helium ions have an initial energy of 5 MeV, and the carbon ions have an initial energy of 100 keV. All ions stop in the chamber gas. For the helium ions, $W = 36$ eV ip^{-1}; for the carbon ions, $W = 48$ eV ip^{-1}. Calculate the saturation current.

12. A source emits 5.16-MeV alpha particles, which are absorbed at a rate of 842 per minute in the gas of a parallel-plate ionization chamber. The saturation current is 3.2×10^{-13} A. Calculate the W value for the alpha particles in the gas.

13. Show that 1 eV ip^{-1} = 1 J C^{-1}.

14. A saturation current of 2.70×10^{-14} A is measured with a parallel-plate ionization chamber in a radiation field. The chamber contains air ($W = 34$ eV ip^{-1}) at 20°C and 752 torr.
- **(a)** What is the rate of energy absorption in the chamber?
- **(b)** If the chamber has a sensitive volume of 750 cm^3, what is the dose rate in the air in J kg^{-1} s^{-1} (= Gy s^{-1})?

15. A parallel-plate ionization chamber is being designed to work with air ($W = 34$ eV ip^{-1}) at STP. When the dose rate in the chamber is 10.0 mGy h^{-1}, the saturation current is to be 10^{-11} A. What volume must the chamber have?

16. Where does most of the gas multiplication occur inside a cylindrical proportional-counter tube?

17. What is the ratio of the pulse heights from a 1-MeV proton ($W = 30$ eV ip^{-1}) and a 1-MeV carbon nucleus ($W = 40$ eV ip^{-1}) absorbed in a proportional counter?

18. Why is a GM counter not useful for determining the absorbed energy in a gas?

19. Show that, at high energies, where the average number of electrons per quantum state is small, the quantum-mechanical distribution Eq. (10.6) approaches the classical Boltzmann distribution, $N = \exp(-E/kT)$.

20. Figure 10.15(b) shows the relative number of electrons at energies E in an intrinsic semiconductor when $T > 0$. Make such a sketch for the As-doped Ge semiconductor shown in Fig. 10.18.

21. What type of semiconductor results when Ge is doped with (a) Sb or (b) In?

22. Make a sketch like that in Fig. 10.17 for Ge doped with Ga (p-type semiconductor).

23. Use the nonrelativistic stopping-power formula and show that Eq. (10.7) holds.

24. What are the relative magnitudes of the responses of an $E(-dE/dx)$ particle identifier to a proton, an alpha particle, and a stripped carbon nucleus?

25. The W value for silicon is 3.6 eV ip^{-1}. Calculate the mean number of ion pairs produced by a 300-keV beta particle absorbed in Si.

26. Calculate the number of ion pairs produced by a 4-MeV alpha particle in

(a) an ionization chamber filled with air ($W = 36$ eV ip^{-1})

(b) a silicon surface-barrier detector ($W = 3.6$ eV ip^{-1}).

27. At a temperature of absolute zero, some electrons occupy states at the donor impurity levels of an n-type semiconductor (Fig. 10.18). True or false?

28. Why is reverse, rather than forward, bias used for semiconductor junctions in radiation measurements?

29. A 1.27-MeV photon loses 540 keV and 210 keV in successive Compton scattering events in the sensitive volume of a Ge detector before escaping.

(a) Estimate the total number of secondary electrons produced by the events.

(b) Would the device register the passage of the photon as a single event or as two events?

30. A silicon semiconductor detector has a dead layer of 1 μm followed by a depletion region 250 μm in depth.

(a) Are these detector dimensions suitable for alpha-particle spectroscopy up to 4 MeV?

(b) For beta-particle spectroscopy up to 500 keV?

31. If 2.1 MeV of absorbed alpha-particle energy produces 41,100 scintillation photons of average wavelength 4800 Å in a scintillator, calculate its efficiency.

32. A 600-keV photon is absorbed in a NaI(Tl) crystal having an efficiency of 11.2%. The average wavelength of the scintillation photons produced is 5340 Å, and 11% of them produce a signal at the cathode of the photomultiplier tube. Calculate the average energy from the incident radiation that produces one photoelectron at the cathode (the "W value").

33. Figure 10.30 was obtained for a 4 × 4 in. NaI(Tl) crystal scintillator. Sketch the observed spectrum if measurements were made with the same source, but with a NaI crystal that was

(a) very large

(b) very small.

(c) In (b), interpret the relative areas under the photopeak and the Compton continuum.

34. In Fig. 10.30, what physical process gives rise to pulses with energies between the Compton edge and the total energy peak?

35. A 1.17-MeV gamma ray is Compton scattered once at an angle of 48° in a scintillator and again at an angle of 112° before escaping.
(a) What (average) pulse height is registered?
(b) If the photon were scattered once at 48° and then photoelectrically absorbed, what pulse height would be registered?

36. The mass attenuation coefficient of NaI (density = 3.67 g cm^{-3}) for 500-keV photons is 0.090 cm^2 g^{-1}. What percentage of normally incident photons interact in a crystal 4 cm thick?

37. Calculate the energy of the backscatter peak for 3-MeV gamma photons.

38. What sequence of events produces the escape peak seen at 11 keV below the total-energy peak when pulse heights from monoenergetic photons are measured with a germanium detector? (See Fig. 10.31.)

39. Calculate the temperature rise in a calorimetric water dosimeter that absorbs 10 J kg^{-1} from a radiation beam (= an absorbed dose of 10 Gy, a lethal dose if given acutely over the whole body). What absorbed dose is required to raise the temperature 1°C?

40. Prove Eq. (10.9).

41. **(a)** Calculate the threshold kinetic energy for an electron to produce Cerenkov radiation in water (index of refraction = 1.33).
(b) What is the threshold energy for a proton?

42. An electron enters a water shield (index of refraction 1.33) with a speed $v = 0.90c$, where c is the speed of light in a vacuum. Assuming that 0.1% of its energy loss is due to Cerenkov radiation as long as this is possible, calculate the number of photons emitted if their average wavelength is 4200 Å.

43. Given the value $Q = 4.78$ MeV for the ^{6}Li(n,α)^{3}H reaction in Table 10.2, calculate T_H and T_{He}.

44. Sketch the pulse-height spectrum from a ^{3}He proportional counter exposed to thermal neutrons. Include wall effects at the appropriate energies.

45. **(a)** What is the maximum energy that a 3-MeV neutron can transfer to a ^{3}He nucleus by elastic scattering?
(b) What is the maximum energy that can be registered in a ^{3}He proportional counter from a 3-MeV neutron?

46. Sketch the pulse-height spectrum from a thin layered boron-lined proportional counter tube for thermal neutrons. Repeat for a layer thicker than the ranges of the reaction products.

47. A proportional-counter tube is lined with a thin coating of a lithium compound (containing ^{6}Li). The tube size and gas pressure are sufficiently large to stop any charged particle that enters the gas. The counter gas is insensitive to thermal neutrons.
- **(a)** Sketch the pulse-height spectrum when the tube is exposed to thermal neutrons. Show the relevant energies and indicate what kind of events produce the signal there.
- **(b)** Repeat for a thick layer of the lithium compound.

48. At what neutron energy is the cross section for the ^{3}He(n,p) reaction equal to the thermal-neutron cross section for the ^{6}Li(n,α) reaction?

49. In the proton-recoil telescope (Fig. 10.46), what is the energy of the scattered neutron if $\theta = 27^\circ$ and $T_p = 1.18$ MeV?

50. Calculate the threshold energy (a) neglecting and (b) including nuclear recoil for the reaction ^{24}Mg(n,p)^{24}Na shown in Table 10.3. The ^{24}Na nucleus is produced in an excited state from which it emits a 1.369-MeV gamma photon and goes to its ground state. (See Appendix D.)

10.10 Answers

1. 3.12×10^5 s^{-1}; 9.33 MeV s^{-1}
2. 1.54×10^5 on average
4. **(a)** 5.00×10^5
(b) 18.0 MeV
(c) 9.29×10^{-9} Gy
5. 1.87×10^{13} eV cm^{-2} s^{-1}
9. **(a)** 236 Bq
(b) 5.29 MeV
(c) 0.101 MeV
11. 2.11×10^{-7} A
15. 95.1 cm^3
24. 1 : 16 : 432
30. **(a)** Yes
(b) No
31. 5.1%
32. 190 eV
35. **(a)** 0.933 MeV
(b) 1.17 MeV
36. 73.3%
39. 0.00239°C; 4180 Gy
41. **(a)** 264 keV
(b) 485 MeV
42. 135
49. 0.31 MeV